Mechanical response of double-network gels with dynamic bonds under multi-cycle deformation

Drozdov, A. D.; deClaville Christiansen, J.

Published in:
Polymer

DOI (link to publication from Publisher):
10.1016/j.polymer.2018.07.020

Publication date:
2018

Document Version
Accepted author manuscript, peer reviewed version

Accepted Manuscript

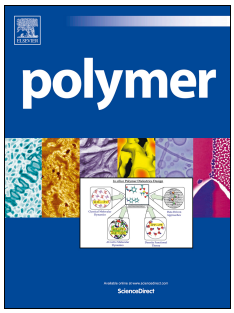

Mechanical response of double-network gels with dynamic bonds under multi-cycle deformation

A.D. Drozdov, J. deClaville Christiansen

PII: S0032-3861(18)30615-3

DOI: 10.1016/j.polymer.2018.07.020

Reference: JPOL 20739

To appear in: *Polymer*

Received Date: 13 April 2018

Revised Date: 7 June 2018

Accepted Date: 4 July 2018

Please cite this article as: Drozdov AD, deClaville Christiansen J, Mechanical response of double-network gels with dynamic bonds under multi-cycle deformation, *Polymer* (2018), doi: 10.1016/j.polymer.2018.07.020.

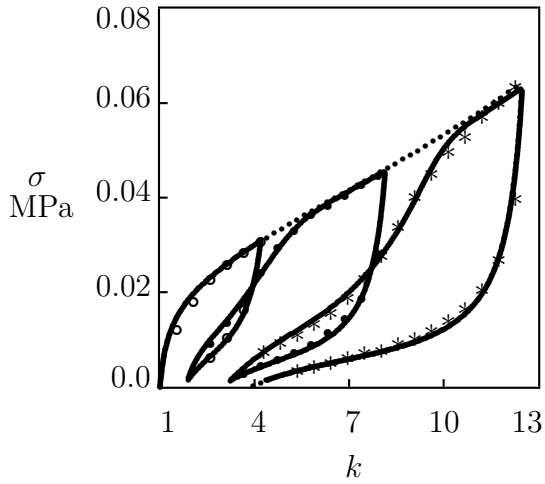

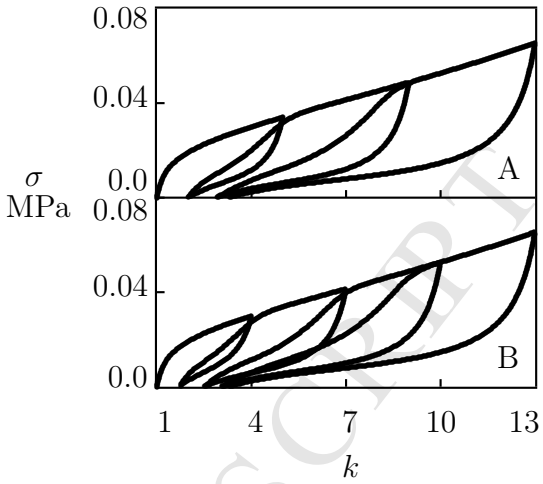

Mechanical response of double-network gels with dynamic bonds under multi-cycle deformation

A.D. Drozdov* and J. deClaville Christiansen
Department of Materials and Production
Aalborg University
Fibigerstraede 16, Aalborg 9220, Denmark

Abstract

Mechanical behavior of double-network (DN) gels with covalent and non-covalent bonds under multi-cycle loading depends strongly on time, strain rate and deformation program. A model is developed for the viscoelastic and viscoplastic responses of a polymer network with permanent and temporary junctions. Viscoelasticity is modeled as breakage and reformation of temporary bonds driven by thermal fluctuations. Viscoplasticity is treated as sliding of permanent junctions with respect to their initial positions in the network. Slippage occurs when a junction becomes unbalanced due to transition of a chain linked by this junction from its active state into the dangling state. Analysis of observations in tensile tests with various strain rates, relaxation tests, loading-unloading tests, and multi-cycle tests with various deformation programs on a series of DN gels shows that the experimental stress–strain diagrams are described correctly by the governing equations, material parameters evolve consistently with experimental conditions, and predictions of the model are in quantitative (where sufficient data are provided) and qualitative agreement with experimental data. In particular, numerical simulation demonstrates the ability of the model to describe the Mullins effect in DN gels.

Key-words: Double-network gel; Cyclic deformation; Mullins effect; Modeling

1 Introduction

Hydrogels are three-dimensional networks of cross-linked hydrophilic chains that swell noticeably being immersed into water. Physical properties of gels resemble those of the native extracellular

*E–mail: aleksey@mp.aau.dk

matrix, which leads to a wide range of their applications in regenerative medicine, tissue engineering, targeted drug delivery, implantable devices, biosensors and soft actificial muscles [1, 2, 3, 4]. Among other applications of pristine and nanocomposite hydrogels, it is worth mentioning their use in energy storage and conversion devices [5]: fuel cells [6, 7, 8], batteries [9], and supercapacitors [10].

Conventional gels with polymer chains bridged by covalent cross-links are relatively weak and brittle [11], which restricts the area of their applications. This shortcoming is explained by the inhomogeneity of a polymer network with randomly distributed chain lengths between cross-links, weak interactions between chains, and the lack of an efficient mechanism for energy dissipation [12].

Strength and toughness of gels can be enhanced significantly by formation of a double-network (DN) structure that involves two inter-penetrating networks of chains [12]. The most promising strategy to prepare polymer networks with superior mechanical properties consists in introduction of sacrificial (dynamic) bonds between chains governed by reversible interactions [13]. Design of DN gels (with chains in a permanent network bridged by chemical cross-links and chains in a transient network bonded by non-covalent junctions) with high stiffness, strength, toughness, and fatigue resistance has recently become a focus of attention [14, 15]. Several mechanisms have been proposed for the development of dynamic bonds in a polymer network [16, 17, 18]: (i) electrostatic interaction (formation of polyion complexes), (ii) metal-ligand coordination, (iii) hydrophobic association, (iv) hydrogen bonding, (v) host-guest recognition, and (vi) reinforcement with nanoparticles.

The mechanical behavior of a covalently cross-linked gel is merely elastic [19]. When temporary bonds are introduced, the response of a gel becomes time- and rate-dependent [20, 21, 22]. The viscoelastic behavior of DN gels can be described [23] within the conventional concept of transient polymer networks where chains with sticky ends detach from and attach to temporary junctions being driven by thermal fluctuations [24, 25]. A constitutive framework for the analysis of the viscoelastic behavior of gels with permanent and temporary junctions has been developed in [26, 27, 28, 29, 30, 31, 32, 33].

Experimental data in multi-cycle tensile (compressive) tests on gels with dynamic bonds reveal two characteristic features:

- Under cyclic deformation with a fixed maximum elongation ratio $k_{\max}$, the hysteresis energy along the first cycle ($n = 1$) exceeds strongly (by an order of magnitude) that measured along subsequent cycles ($n > 1$). For all $n \geq 2$, this energy decreases weakly with number of cycles and becomes practically independent of n after a few cycles of loading–retraction [34, 35, 36].

- (ii) When cyclic deformation is conducted with monotonically increasing elongation ratios,

the stress–strain diagram under reloading along the $(n+1)$th cycle coincides with that under uniaxial tension, provided that the elongation ratio k exceeds sufficiently the maximum elongation ratio at the nth cycle (the Mullins effect) [37, 38, 39].

Constitutive equations for the viscoelastic and viscoplastic behavior of DN gels under cyclic loading have recently been developed in [30, 40, 41, 42, 43]. Although these models capture the mechanical response of gels with covalent and non-covalent junctions, discrepancies can be observed between experimental data and results of simulation. This is not surprising as the above models treat some phenomena (viscoelasticity, viscoplasticity, damage accumulation, etc.) in a simplified manner.

The objective of the present study is threefold: (i) to develop a model for the mechanical behavior of DN gels under cyclic deformation that accounts adequately for their time- and rate-dependent responses, (ii) to determine adjustable parameters by fitting observations in tensile tests with various strain rates, relaxation tests, and cyclic tests, and (iii) to demonstrate the ability of the model to predict observations in multi-cycle tests with various deformation programs and arbitrary strains, at which the strain rate changes its sign.

This work focuses on the response of DN gels in tests with a reasonably small number of cycles (low-cycle fatigue) being driven by possible applications of these materials in shock-absorbing medical devices [44, 45].

An equivalent polymer network in a DN gel is treated as a combination of permanent and transient networks. Dissipation of energy is induced by two processes: (i) breakage and reformation of temporary bonds between chains driven by thermal fluctuations (viscoelasticity), and (ii) slippage of permanent cross-links with respect to their reference positions (viscoplasticity).

The former mechanism for energy dissipation is conventional for transient networks, where a dangling chain adopts the actual state of a gel at the instant of its reattachment as the reference (stress-free) state. The describe observations in relaxation tests (which requires the entire spectrum of relaxation times [21, 46] to be accounted for), we adopt the approach of [47, 48] and presume the equivalent network to be heterogeneous and composed of meso-domains with various activation energies for rearrangement of chains.

The latter mechanism for dissipation was recently suggested in [49]. According to it, a junction between chains becomes unbalanced when one of the chains connected by this junction is transformed from the active state into the dangling state (which means that stress in this chain vanishes suddenly). As a result, the junction begins to slide with respect to the network (plastic flow) until

it reaches a new equilibrium state.

The novelty of our approach consists in (i) the description of both phenomena (viscoelasticity and viscoplasticity) within a unified constitutive model grounded on the free energy imbalance inequality and (ii) the account for two (dissipative and non-dissipative) mechanisms for plastic flow of permanent junctions.

The ability of the model to describe observations is confirmed by matching experimental data on (i) poly(vinyl alcohol) gel, where chains are chemically cross-linked with glutaraldehyde and physically cross-linked with borate ions [27, 29, 50], (ii) poly(N,N-dimethylacrylamide) gel reinforced with silica nanoparticles [51], (iii) poly(acrylamide–co-2-acrylamido-2-methyl propane sulfonic acid) gel loaded with zirconium hydroxide nanoparticles [52], (iv) poly(N,N-dimethylacrylamide) [53] and poly(N-isopropylacrylamide) [54] gels reinforced with nanoclay, (v) poly(acrylamide–acrylic acid) gel cross-linked with hydrophobic aggregates and Fe^{3+} ions [55, 56], (vi) poly(acrylamide–n-dodecyl glyceryl itaconate) (AAm-DGI) gel, where DGI bilayers are connected with a covalently cross-linked AAm matrix by hydrogen bonds [57, 58], and (vii) poly(acrylamide-alginate) (AAm-Alg) gel with covalently cross-linked AAm chains and ionically cross-linked Alg chains [59].

2 Model

A gel is treated as a two-phase medium composed of an equivalent polymer network and water molecules. The solid and fluid phases are modeled as immiscible interpenetrating continua. Deformation of the network and concentration of water molecules are connected by the molecular incompressibility condition.

The polymer network is thought of as a superposition of two networks: permanent and transient. Chains in the former network are bonded by permanent junctions, while chains in the latter network are bridged by temporary junctions that rearrange (break and reform) being driven by thermal fluctuations. According to the affinity hypothesis, deformations of the permanent and transient networks coincide with macro-deformation of the gel.

The reference (stress-free) state of the permanent network before application of external loads coincides with the as-prepared state of the gel. According to the multiplicative decomposition formula, the deformation gradient $\mathbf{F}$ for transition from the initial (undeformed dry) state into the actual (deformed swollen) state is given by

$$\mathbf{F} = \mathbf{F}_{\mathrm{e}} \cdot \mathbf{F}_{\mathrm{p}}, \tag{1}$$

where $\mathbf{F}_\mathrm{e}$ and $\mathbf{F}_\mathrm{p}$ are the deformation gradients for elastic and plastic deformations, and the dot stands for inner product. Under the conventional hypothesis that the plastic spin vanishes, the rate-of-strain tensors for plastic deformation ($\mathbf{d}_\mathrm{p}$ in the unloaded state and $\mathbf{D}_\mathrm{p}$ is the actual state) read

$$\mathbf{d}_\mathrm{p} = \dot{\mathbf{F}}_\mathrm{p} \cdot \mathbf{F}_\mathrm{p}^{-1}, \qquad \mathbf{D}_\mathrm{p} = \frac{1}{2}\Big(\mathbf{F}_\mathrm{e} \cdot \mathbf{d}_\mathrm{p} \cdot \mathbf{F}_\mathrm{e}^{-1} + \mathbf{F}_\mathrm{e}^{-\top} \cdot \mathbf{d}_\mathrm{p} \cdot \mathbf{F}_\mathrm{e}^{\top}\Big), \tag{2}$$

where the superscript dot stands for the derivative with respect to time, and $\top$ denotes transpose.

Following [60], two mechanisms of plastic deformation (sliding of junctions between chains with respect to their initial positions) are introduced: (i) induced by macro-deformation (with the rate-of-strain tensor $\mathbf{d}_\mathrm{m}$) and (ii) driven by inter-chain interaction (with the rate-of-strain tensor $\mathbf{d}_\mathrm{i}$). The rate-of-strain tensor for plastic deformation is determined by

$$\mathbf{d}_\mathrm{p} = \mathbf{d}_\mathrm{m} + \mathbf{d}_\mathrm{i}. \tag{3}$$

The rate-of-strain tensor $\mathbf{D}_\mathrm{m}$ (an analog of $\mathbf{d}_\mathrm{m}$ in the actual state) is proportional to the rate-of-strain tensor for macro-deformation

$$\mathbf{D}_\mathrm{m} = \phi \mathbf{D}. \tag{4}$$

The non-negative coefficient ϕ in Eq. (4) vanishes in the initial state (sliding of junctions is negligible at infinitesimal strains), increases under tension (which accelerates the sliding process) and tends to its ultimate value $\phi = 1$ at large elongation ratios. Evolution of the function ϕ with time is governed by the equation

$$\dot{\phi} = \pm A(1-\phi)^2, \qquad \phi(0) = 0. \tag{5}$$

The signs "+" in Eq. (5) corresponds to loading, the sign "−" corresponds to unloading, and the right-hand side of Eq. (5) vanishes when the strain rate for macro-deformation equals zero. The coefficient A reads

$$A = \frac{a}{(I_1 - 2)^{\frac{3}{2}}}, \tag{6}$$

where a is a positive adjustable parameter, and I_1 is the first principal invariant of the Cauchy–Green tensor for macro-deformation. Under uniaxial tension with elongation ratio k, the presence of $I_1 = k^2 + 2/k$ in the denominator in Eq. (6) ensures that $\dot{\phi}$ remains small at large elongation ratios. Eqs. (5) and (6) differ from the kinetic equations introduced in [61, 62].

To describe the response of a transient network, we denote by τ an instant when an active chain (both ends are connected to the network) is bridged with the network by a temporary junction, and distinguish chains that joined the network under polymerization of a pre-gel solution ($\tau = 0$)

and those attaching the network under deformation ($\tau > 0$). The reference (stress-free) state of a chain with $\tau = 0$ coincides with the as-prepared state of the gel. The reference state of a chain with $\tau > 0$ coincides with the actual state of the gel at instant τ (stresses in chains totally relax under rearrangement).

With reference to [22], the transient network is presumed to be inhomogeneous and composited of meso-domains with various activation energies U for breakage of temporary bonds. The non-homogeneity is described by the distribution function $f(u)$ of meso-domains with dimensionless activation energies $u = U/(k_{\mathrm{B}}T)$, where k_{B} is the Boltzmann constant, and T stands for the absolute temperature. The quasi-Gaussian expression is adopted for this function

$$f(u) = f_0 \exp\Big(-\frac{u^2}{2\Sigma^2}\Big) \qquad (u \geq 0), \tag{7}$$

where $\Sigma > 0$ is a material constant, and the coefficient f_0 is determined from the normalization condition $\int_0^\infty f(u)\mathrm{d}u = 0$. Rearrangement of the inhomogeneous network is entirely determined by the rate of detachment of active chains from temporary junctions

$$\Gamma = \gamma \exp(-u), \tag{8}$$

where $\gamma > 0$ stands for the attempt rate.

Constitutive equations for the mechanical response of a DN gel under an arbitrary deformation with finite strains are developed in Supporting Information. These relations are derived by means of the free energy imbalance inequality for an arbitrary specific mechanical energy of the permanent network

$$W_{\mathrm{e}}(I_{\mathrm{e}1}, I_{\mathrm{e}2}, I_{\mathrm{e}3}) + W_{\mathrm{i}}(I_{\mathrm{i}1}, I_{\mathrm{i}2})$$

and an arbitrary strain energy of chain in the transient network

$$w(I_{\tau 1}, I_{\tau 2}, I_{\tau 3}).$$

The specific energy W_{e} stored in chains of the permanent network depends on the principal invariants $I_{\mathrm{e}m}$ ($m = 1, 2, 3$) of the Cauchy–Green tensor for elastic deformation $\mathbf{B}_{\mathrm{e}} = \mathbf{F}_{\mathrm{e}} \cdot \mathbf{F}_{\mathrm{e}}^{\top}$. The specific energy of inter-chain interaction W_{i} is treated as a function of the principal invariants $I_{\mathrm{i}m}$ ($m = 1, 2$) of the Cauchy–Green tensor for plastic deformation $\mathbf{B}_{\mathrm{i}} = \mathbf{F}_{\mathrm{i}} \cdot \mathbf{F}_{\mathrm{i}}^{\top}$. The energy w stored in an active chain of the transient network is presumed to depend on the principal invariants $I_{\tau m}$ ($m = 1, 2, 3$) of the Cauchy–Green tensor $\mathbf{b}_\tau = \mathbf{f}_\tau \cdot \mathbf{f}_\tau^{\top}$, where $\mathbf{f}_\tau(t) = \mathbf{F}(t) \cdot \mathbf{F}^{-1}(\tau)$ is the deformation gradient for transition from the actual state at time τ to the actual state at time t.

In the analysis of observations, we focus on uniaxial tensile cyclic deformation of a gel with the strain energy density of the permanent network

$$W_{\rm e} = -\frac{1}{2}G_{\rm e}\Big[K\ln\Big(1-\frac{I_{\rm e1}-3}{K}\Big)+\ln I_{\rm e3}\Big], \tag{9}$$

the energy of inter-chain interactions

$$W_{\rm i} = \frac{1}{2}G_{\rm i}(I_{\rm i1}-3), \tag{10}$$

and the energy of active chains in the transient network

$$w = \frac{1}{2}g\Big[(I_{\tau 1}-3)-\ln I_{\tau 3}\Big], \tag{11}$$

where $G_{\rm e}$, $G_{\rm i}$, g and K are constants.

The Gent equation (9) is adopted for the function $W_{\rm e}$ to account for strain-hardening of DN gels at large elongation ratios [63]. The energy of inter-chain interaction $W_{\rm i}$ is accepted in the neo-Hookean form (10), which serves as the first term in the formal expansion of the function $W_{\rm i}$ into the Taylor series with respect to its arguments. Eq. (11) was developed in [64] within the concept of entropic elasticity.

Governing equations for a DN gel equilibrated before loading and subjected to uniaxial tensile cyclic deformation with a constant strain rate $\dot\epsilon$ involve

(i) the formula for engineering tensile stress

$$\sigma = G\Big[(1-\kappa)(1-\phi)V\frac{k_{\rm e}^3-1}{kk_{\rm e}}+\kappa\Big(S_1k-\frac{S_2}{k^2}\Big)\Big], \tag{12}$$

where the coefficient

$$V = \Big[1-\frac{1}{K}\Big(k_{\rm e}^2+\frac{2}{k_{\rm e}}-3\Big)\Big]^{-1}$$

accounts for stress-hardening,

(ii) the kinematic equation for elongation ratio k under macro-deformation

$$\dot k = \pm\dot\epsilon, \qquad k(0)=1, \tag{13}$$

(iii) the kinematic equation for elongation ratio $k_{\rm e}$ for elastic deformation

$$\frac{\dot k_{\rm e}}{k_{\rm e}} = (1-\phi)\frac{\dot k}{k}-\frac{\dot k_{\rm i}}{k_{\rm i}}, \qquad k_{\rm e}(0)=1, \tag{14}$$

(iv) the kinetic equation for elongation ratio $k_{\rm i}$ under plastic deformation

$$\frac{\dot k_{\rm i}}{k_{\rm i}} = P\Big(V\frac{k_{\rm e}^3-1}{k_{\rm e}}-R\frac{k_{\rm i}^3-1}{k_{\rm i}}\Big), \qquad k_{\rm i}(0)=1, \tag{15}$$

(v) the integral relations for the functions S_1 and S_2

$$S_1 = \int_0^\infty f(u)s_1(t,u)\mathrm{d}u, \qquad S_2 = \int_0^\infty f(u)s_2(t,u)\mathrm{d}u, \tag{16}$$

(vi) the kinetic equations for the functions s_1 and s_2

$$\frac{\partial s_1}{\partial t} = \Gamma\Big(\frac{1}{k^2} - s_1\Big), \qquad \frac{\partial s_2}{\partial t} = \Gamma(k - s_2), \qquad s_1(0,u) = s_2(0,u) = 1. \tag{17}$$

Eqs. (12)–(17) together with Eqs. (5)–(9) contain five material constants: G stands for the elastic modulus of a gel, K^{-1} is the Gent constant [65], κ denotes the ratio of elastic moduli of transient and permanent networks, a characterizes plastic flow of junctions induced by macro-deformation, and Σ is a measure of inhomogeneity of the transient network.

The governing equations involve three adjustable functions: γ, P and R.

Parameter γ denotes the attempt rate for separation of chains from temporary junctions. To describe the nonlinear viscoelastic behavior of DN gels, we presume this quantity to be affected by dissipative plastic flow. The following relation is adopted for this dependence:

$$\gamma = \gamma_* \exp\Big[-\alpha(I_{\mathrm{i}2} - 3)\Big], \tag{18}$$

where γ_* is the attempt rate at infinitesimal strains, the constant α describes changes in the rate of rearrangement, and $I_{\mathrm{i}2}$ is the second principal invariant of the Cauchy–Green tensor $\mathbf{B}_{\mathrm{i}}$.

Coefficient P determines the rate of sliding of junctions driven by inter-chain interaction, and parameter R stands for the ratio of moduli G_{i} and G_{e} that characterize mechanical energies dissipated by and stored in the permanent network.

In the analysis of multi-cycle deformation, three regimes are distinguished: (i) stretching of a virgin sample ($\dot{k} > 0$), (ii) retraction ($\dot{k} < 0$), and (iii) reloading ($\dot{k} > 0$). Parameter P is presumed to vanish under stretching and stress relaxation ($\dot{k} = 0$), and to accept different values, P_1 and P_2, under retraction and reloading:

$$P = 0 \quad \text{(stretching)}, \qquad P = P_1 \quad \text{(retraction)}, \qquad P = P_2 \quad \text{(reloading)}. \tag{19}$$

The rate of plastic flow under retraction is determined by the formula

$$P_1 = P_{1*} \exp\Big[\beta_1(\sigma_* - \sigma)\Big]. \tag{20}$$

Here P_{1*} is the rate of sliding of junctions at the instant when unloading starts and tensile stress equals its maximum value σ_*, and the constant β_1 accounts for slowing down of the sliding process driven by the decay in tensile stress.

The rate of plastic flow under reloading is given by the equation

$$P_2 = P_{2*} \exp\Big[\beta_2(\sigma - \sigma_*)\Big], \tag{21}$$

where P_{2*} is the rate of sliding of junctions at the instant when retraction starts and tensile stress equals its minimum value σ_*, and the constant β_2 accounts for stress-induced acceleration of the sliding process.

By analogy with Eq. (19), the coefficient R is presumed to accept different values under retraction and reloading

$$R = R_1 \quad \text{(retraction)}, \qquad R = R_2 \quad \text{(reloading)}. \tag{22}$$

Coefficients P_{1*}, P_{2*}, R_1, R_2, β_1, β_2 remain constant along each retraction and reloading path, but they may be affected by elongation ratios $k_{\max}$ and $k_{\min}$, at which unloading and reloading occur. Evolution of these quantities with $k_{\max}$ and $k_{\min}$ reflects damage accumulation (changes in the micro-structure of DN gels) under multi-cycle deformation.

To reduce the number of phenomenological relations in the model, we postulate that β_1 and R_2 are material constants independent of $k_{\max}$ and $k_{\min}$, respectively. Changes in the remaining parameters P_{1*}, R_1, P_{2*}, β_2 are described by the equations

$$\log P_{1*} = P_{1*}^0 + P_{1*}^1(I_{\mathrm{e}2} - 3), \qquad \log R_1 = R_1^0 + R_1^1(I_{\mathrm{e}2} - 3), \tag{23}$$

$$\log P_{2*} = P_{2*}^0 + P_{2*}^1(I_{\mathrm{i}2} - 3), \qquad \log \beta_2 = \beta_2^0 + \beta_2^1(I_{\mathrm{i}2} - 3), \tag{24}$$

where $\log = \log_{10}$, the principal invariants of the Cauchy–Green tensors for elastic $I_{\mathrm{e}2} = 2k_{\mathrm{e}} + k_{\mathrm{e}}^{-2}$ and plastic $I_{\mathrm{i}2} = 2k_{\mathrm{i}} + k_{\mathrm{i}}^{-2}$ deformations are calculated at the points where the strain rate $\dot{\epsilon}$ changes its sign, and the coefficients are determined by the least-squares method.

An advantage of the constitutive model is its ability to describe correctly experimental stress–strain diagrams of DN gels under multi-cycle deformations with arbitrary programs (elongation ratios $k_{\max}$ and $k_{\min}$ at which the strain rate changes its sign). To reach this goal, mutual dependencies are introduced between stresses and plastic flow (Eqs. (20), (21)) and between viscoelastic and viscoplastic responses (Eq. (18)). As a result, the number of material constants increases. Although this number is not small, it remains lower than the number of adjustable parameters in other models for the viscoelastic and viscoplastic response of DN gels under cyclic deformation.

3 Fitting of observations

In this section, the ability of the constitutive model is verified to describe experimental stress–strain diagrams on DN gels under various deformation programs.

3.1 Time- and rate-dependent behavior

First, we demonstrate that the governing equations with a fixed set of material parameters describe correctly observations in tensile tests with various strain rates, relaxation tests and loading–unloading tests.

We begin with the analysis of observations on PVA gel synthesized by means of a two-stage procedure [27]. At the first stage, PVA chains in an aqueous solution (12 wt.%, molecular weight 89 to 98 kg/mol) were covalently cross-linked with glutaraldehyde (molar fraction 5.5 mM) under acidic condition (pH=1.7) at 100 °C . After washing in deionized water, the swollen gel was immersed into an aqueous solution of sodium tetraborate decahydrate (1 mM) and sodium chloride (90 mM) for 3 days. The first network is formed by polymer chains bridged by chemical cross-links. In the other network, chains are linked by physical bonds between hydroxyl groups of PVA and borate ions (due to di-diol complexation [66] and formation of ionic and hydrogen bonds [67]).

Mechanical tests were conducted on as-prepared specimens with degree of swelling $Q_0 = 8.3$. The experimental program involves: (i) a tensile relaxation test with elongation ratio $k_{\max} = 1.1$ and strain rate under stretching $\dot{\epsilon} = 0.2$ s^{-1}, (ii) a series of tensile tests with maximum elongation ratio $k_{\max} = 2$ and various strain rates $\dot{\epsilon}$ ranging from 0.003 to 0.1 s^{-1}, (iii) two series of cyclic (loading–unloading) tests with maximum elongation ratio $k_{\max} = 1.3$, strain rates under stretching $\dot{\epsilon}_1 = 0.01$ and 0.3 s^{-1} and strain rates under retraction $\dot{\epsilon}_2 = 0.001$, 0.01 and 0.1 s^{-1}, and (iv) a cyclic test with maximum elongation ratio $k_{\max} = 2$ and strain rate $\dot{\epsilon} = 0.03$ s^{-1}. Observations in these tests are chosen because the amount of experimental data is sufficient to determine material constants and to examine accuracy of the model predictions.

To determine adjustable parameters, we start with matching observations in the relaxation test with $k_{\max} = 1.1$ (Fig. 1A). As the strain $k_{\max} - 1$ is small, the data are fitted by means of Eq. (S-92) (Supporting Information), where parameters κ, γ_* and Σ are found by the method of nonlinear regression. Then the stress–strain diagram is matched under tension with strain rate $\dot{\epsilon} = 0.01$ s^{-1} (Fig. 1B). We set $K = \infty$ (the influence of the Gent constant is negligible at elongation ratios $k < 2$), and determine coefficients G and a from the best-fit condition. The values of material

constants are listed in Tab. S1. In particular, we set $P_{1*} = 0$, which means that the dissipative mechanism of plasticity is disregarded.

To demonstrate validity of the constitutive equations, predictions of the model are compared with experimental data. First, the response of PVA gel in relaxation test is studied (with account for the finite strain rate $\dot{\epsilon}$ under tension). Results are depicted in Fig. S1, which shows the stress–strain diagram under stretching and the decay in stress with time under relaxation. Secondly, numerical analysis is conducted of the response of PVA gel in tensile tests with various strain rates $\dot{\epsilon}$. Its results are reported in Fig. 1B. Finally, simulation is performed of the rate-dependent behavior in cyclic (loading–unloading) tests with various strain rates and maximum elongation ratios. Results of numerical analysis are presented in Figs. 2 and S2.

We proceed with fitting observations on poly(N, N-dimethylacrylamide) (DMA) gel reinforced with silica nanoparticles (NP) [51]. The gel was prepared by free-radical polymerization (12 h at 25 °C) of DMA monomers (1.485 g) in a suspension of silica NP (0.74 g, average radius 17 nm) in water (10.44 g) by using potassium persulfate (KPS, 0.041 g) as an initiator and N, N, N', N'-tetramethylethylenediamine (TEMED, 0.017 g) as a catalyst. The first network in the DN gel is formed due to self-crosslinking of polymer chains driven by chemical reaction between KPS and methyl groups of DMA [51]. The other network is formed by physical bonds between polymer chains and nanoparticles.

Mechanical tests were conducted on as-prepared specimens with degree of swelling $Q_0 = 8.4$. The experimental program involves: (i) a tensile relaxation test at elongation ratio $k_{\max} = 1.5$ and strain rate under stretching $\dot{\epsilon} = 0.06$ s^{-1}, and (ii) a cyclic test with maximum elongation ratio $k_{\max} = 6$ and strain rate $\dot{\epsilon} = 0.06$ s^{-1} under tension and retraction. Observations are depicted in Fig. 3 together with results of numerical simulation with the material constants collected in Tab. S2.

To determine adjustable parameters in the governing equations, the above procedure is slightly modified (it cannot be applied directly because tensile strain in the relaxation test is not small). First, γ_* and Σ are determined by matching observations in the relaxation test with the help of Eq. (S-92). Given κ, parameters G and K are found by fitting experimental data under tension in the cyclic test with $k_{\max} = 6$ (results of simulation show that $a_* = 0$). Then κ is calculated from the best-fit condition for observations in the relaxation test. Finally, we set $\alpha = 0$ and fit experimental data under retraction to determine P_{1*}, R_1 and β_1.

We now study observations on poly(N, N-dimethylacrylamide) (DMA) gel reinforced with nan-

oclay (NC) [53]. The gel was prepared by free radical polymerization (55 h at room temperature) of DMA monomers (4 ml) in a suspension of Laponite XLS nanoclay (1.8 g) in water (19.5 ml) by using an aqueous solution of KPS (2 ml) as an initiator and TEMED (30 μl) as a catalyst. The double-network structure of DMA-NC gel involves entangled DMA chains linked with clay particles by physical bonds (the first network) and weakly charged exfoliated clay platelets bridged by electrostatic interaction (the other network).

Mechanical tests were conducted on as-prepared specimens with degree of swelling $Q_0 = 3.7$. The experimental program involves: (i) a tensile relaxation test at elongation ratio $k_{\max} = 2$ and strain rate under stretching $\dot{\epsilon} = 0.5$ s^{-1}, and (ii) a cyclic test with maximum elongation ratio $k_{\max} = 6$ and strain rate $\dot{\epsilon} = 0.06$ s^{-1} under tension and retraction. Observations in these tests are depicted in Fig. 4 together with results of numerical simulation. Material constants determined by the above procedure are collected in Tab. S3.

An advantage of our model compared with the models developed in [27, 29] (where observations on PVA gel were fitted) consists in its simplicity: the governing relations involve differential equations only, which means that no special procedures are required for numerical solution of nonlinear integral equations. Its advantage compared with the model derived in [30] (where experimental data in cyclic tests on DMA-NP and DMA-NC gels were analyzed) consists in the account for the time- and rate-dependent response and higher quality of fitting observations (due to the account for two mechanisms of plastic flow).

The following conclusions are drawn:

(I) Good agreement is demonstrated between results of simulation and observations in tensile tests with various strain rates, relaxation tests and loading-unloading tests (Figs. 1, 3, 4 and S1A).

(II) The model predicts quantitatively experimental data in loading–retraction tests with various strain rates when its parameters are determined by matching observations in independent experiments (Figs. 2 and S2).

3.2 Cyclic tests with various maximum elongation ratios

Our aim now is (i) to demonstrate that the response of DN gels in loading–unloading tests with various maximum elongation ratios $k_{\max}$ is described adequately by Eq. (23) and (ii) to assess how intensity of stress relaxation is affected by $k_{\max}$.

We begin with fitting observations on poly(acrylamide–acrylic acid–*n*-octadecyl acrylate) (AAm-AAc-ODA) gel prepared by means of a three-stage procedure [55]. At the first stage, micellar

copolymerization was performed (12 h at 65 °C) of AAm monomers (12 wt.%), AAc monomers (10 wt.% of AAm) and ODA monomers (35 wt.% of AAm) in an aqueous solution of ionic surfactant sodium dodecyl sulfate (SDS, 18 wt.%) and sodium chloride (1.5 M) by using ammonium persulfate (APS, 1 wt.%) as an initiator. After polymerization, the gel was soaked in distilled water at room temperature to extract SDS and residual monomers. At the other stage, the gel samples were immersed for 24 h in an aqueous solution of iron chloride hexahydrate $FeCl_3 \cdot 6H_2O$ (50 mM). At the final stage, the samples were rinsed in deionized water for 48 h to remove superfluous Fe^{3+} ions. The first network is formed by polymer chains linked by hydrophobic aggregates of ODA, while the other network is developed due to bonding of chains by ion complexes between mobile Fe^{3+} cations and fixed COO^- anions.

Mechanical tests were conducted on fully swollen specimens with degree of swelling $Q_0 = 2.6$. Tensile cyclic tests were performed with a constant strain rate $\dot{\epsilon} = 0.083\ s^{-1}$ and various maximum elongation ratios k_{max} ranging from 2 to 6. Observations in these tests are depicted in Fig. 5 together with results of numerical simulation with the material parameters listed in Tab. S4.

Bearing in mind that observations on the time-dependent response were not provided, we determine constants γ_*, Σ and κ together with G and a by matching the loading path of the stress–strain diagram with $k_{max} = 6$ (we set $K = \infty$ to reduce the number of adjustable parameters). Then we set $\alpha = 0$ and determine P_{1*}, R_1 and β_1 by fitting observations under retraction in the test with $k_{max} = 6$. Finally, we fix β_1 and approximate experimental data under unloading in cyclic tests with other k_{max} by means of two parameters, P_{1*} and R_1. Evolution of these quantities with maximum elongation ratio k_{max} is illustrated in Fig. S3, where the data are approximated by Eq. (23).

We proceed with study of a similar DN gel whose chains are linked by hydrophobic aggregates and ion complexes [56]. Poly(acrylamide–acrylic acid–stearyl methacrylate) (AAm-AAc-SMA) gel was synthesized in a three-stage process. At the first stage, micellar polymerization was conducted of AAm monomers (17.4 wt.%), AAc monomers (15 mol.% of AAm) and hydrophobic SMA monomers (1 mol.% of AAm) in an aqueous solution of SDS and sodium chloride (0.8 M) by using Irgacure-2959 (1 mol.% of monomers) as a photo-initiator. A gel with physical cross-links formed by poly(stearyl methacrylate) blocks inside SDS micelles was prepared by photo-polymerization of the pre-gel solution (2 h under UV light). At the other stage, this gel was immersed for 16 h in a solution of iron chloride hexahydrate (50 mM) at room temperature to form ionic complexes between Fe^{3+} cations and carboxyl groups of AAc. Finally, the samples were soaked in deionized

water for 3 days to extract SDS, residual monomers and superfluous Fe^{3+} ions and to reorganize the structure of metal coordination bonds.

Tensile loading–unloading tests were performed on as-prepared specimens with an unspecified degree of swelling with strain rate $\dot{\epsilon} = 0.167$ s^{-1} and various maximum elongation ratios $k_{\max}$ ranging from 1.5 to 6. Observations in these tests are depicted in Fig. 6 together with results of numerical simulation with the material parameters collected in Tab. S4. Each retraction curve in Fig. 6 is characterized by two parameters, P_{1*} and R_1. The effect of $k_{\max}$ on these quantities is illustrated in Fig. S4 where the data are approximated by Eq. (23).

Tab. S3 shows that material parameters of these gels adopt similar values (the only exception from this rule is Σ whose value for AAm-AAc-ODA gel exceeds that for AAm-AAc-SMA gel by a factor of 3.5). Figs. S3 and S4 demonstrate that the effect of maximum elongation ratio $k_{\max}$ on adjustable parameters P_{1*} and R_1 is weakly affected by the chemistry of hydrophobic aggregates and preparation conditions. The coefficients P_{1*}^1 coincide for the gels (they equal -0.21), while the coefficients R_1^1 are close to each other (-0.27 for AAm-AAc-ODA and -0.15 for AAm-AAc–SMA).

To evaluate the effect of Σ, which characterizes width of the relaxation spectrum $f(u)$, on the time-dependent behavior of AAm-AAc-ODA and AAm-AAc–SMA gels, numerical analysis is performed of their response in relaxation tests. In simulation, a sample is stretched with a fixed strain rate $\dot{\epsilon}$ up to the elongation ratio $k_{\max}$, which remains fixed during the period of relaxation. Results of calculations are depicted in Figs. S5 and S6, where the ratio of tensile stresses $S = \sigma(t_{\rm rel})/\sigma_0$ is plotted versus relaxation time $t_{\rm rel}$ (σ_0 is the stress at the instant t_0 when relaxation starts, and $t_{\rm rel} = t - t_0$). These figures show that S decreases monotonically with $t_{\rm rel}$ at each $k_{\max}$ and reaches its ultimate value within a few minutes. The duration of the transition period is strongly affected by Σ: it equals about 100 s for AAm-AAc-ODA gel (large Σ) and about 40 s for AAm-AAc–SMA gel (small Σ). Given relaxation time $t_{\rm rel}$, the intensity of stress relaxation $1 - S$ decreases monotonically with $k_{\max}$ and becomes negligible at relatively large elongation ratios. The latter conclusion is in accord with observations reported in [68].

We now approximate experimental data in cyclic tests on poly(acrylamide–*n*-dodecyl glyceryl itaconate) (AAm–DGI) gel [57]. The gel was prepared by cross-linking polymerization at room temperature of AAm monomers (2 M) and amphiphilic DGI monomers (with two molar fractions 0.1 M and 0.13 M) in an aqueous solution of SDS (0.025 mol.% with respect to DGI) by using N, N'-methylenebisacrylamide (BIS, 2 mM) as a cross-linker and Irgacure (2 mM) as an initiator. In the presence of SDS, DGI forms lamellar bilayers homogeneously distributed in the AAm network and

connected to the matrix by hydrogen bonds. The dual-network structure is formed by AAm chains covalently cross-linked with BIS (the first network) and DGI lamellar bilayers physically bonded with AAm chains (the other network).

Experiments were conducted on as-prepared specimens with degree of swelling $Q_0 = 16.9$. Cyclic tests were performed with strain rate $\dot{\epsilon} = 0.005$ s^{-1} and various maximum elongation ratios $k_{\max}$ ranging from 2 to 7. Observations in these tests on AAm-DGI gel with 0.13 M of DGI in the pre-gel solution are depicted in Fig. 7 together with results of simulation with the material parameters collected in Tab. S5. The effect of $k_{\max}$ on parameters P_{1*} and R_1 (that characterize plastic flow under retraction) is illustrated in Fig. S7, where the data are fitted by means of Eq. (23).

The stress–strain curve in Fig. 7 involves an interval of stress-softening under stretching (along which the engineering stress remains practically independent of elongation ratio) followed by a pronounced increase in σ at large k. A similar diagram that shows a non-monotonic stress–strain dependence under tension is presented in Fig. 8, where observations on the gel with 0.1 M of DGI are depicted (cyclic test with strain rate $\dot{\epsilon} = 0.005$ s^{-1} and maximum elongation ratio $k_{\max} = 4$) together with results of simulation. Analogous stress–strain curves were reported on poly(N, N-dimethylacrylamide-co-methacrylic acid) gel [69], AAm-agar gels with relatively high concentrations of agar in pre-gel solutions [70], and poly(3-(methacryloylamino)propyl-trimethylammonium chloride-co-sodium p-styrenesulfonate) gel [71, 72]. In accord with [69], the model describes these phenomena as a competition between non-dissipative plastic flow under stretching (characterized by parameter a) and the non-Gaussian response of polymer chains (determined by the constant K). Tab. S5 shows that stress-softening corresponds to small a and large K values, whereas the non-monotonicity of the stress–strain curve is observed at large a and relatively small K values. Another explanation for stress-softening of DN gels was provided in [30, 40], where it was associated with necking instability under tension.

To examine how non-monotonicity of the stress–strain diagram on a DN gel affects its time-dependent behavior, simulation is conducted of the responses of AAm–DGI gels with 0.1 M and 0.13 M of DGI in relaxation tests with various maximum elongation ratios $k_{\max}$. Results of calculations are reported in Fig. S8, where the dimensionless ratio S is plotted versus relaxation time $t_{\rm rel}$. This figure shows that for any $t_{\rm rel}$, the intensity of stress relaxation $1 - S$ decreases monotonically with $k_{\max}$ (including the interval of $k_{\max}$ values, where the stress σ remains constant or decreases with elongation ratio). Comparison of Figs. S5, S6 and S8 reveals that the characteristic time for stress

relaxation in AAm–DGI gels exceeds pronouncedly that in AAm-AAc-ODA and AAm-AAc-SMA gels. This reflects the fact that γ_* of the former gels is lower than that of the latter gels by an order of magnitude.

The following conclusions are drawn:

(I) The model describes correctly stress–strain diagrams on DN gels under cyclic loading with various maximum elongation ratios (Figs. 5 to 8).

(II) The response under retraction is uniquely determined by two parameters, P_{1*} and R_1. Evolution of these quantities with $k_{\max}$ is described by Eq. (23) (Figs. S3, S4 and S7).

(III) The intensity of stress relaxation increases with relaxation time $t_{\rm rel}$ and decreases with elongation ratio $k_{\max}$ at which the test is conducted (Figs. S5, S6 and S8).

3.3 The Mullins effect

The ability of the model is now verified to describe observations in multi-cycle tensile tests with two deformation programs: (i) oscillations between fixed maximum elongation ratio under stretching $k_{\max}$ and minimum stress under retraction $\sigma_{\min}$, and (ii) oscillations with monotonically increasing maximum elongation ratios $k_{\max\, n}$ and a fixed stress under retraction $\sigma_{\min}$.

We begin with the analysis of observations on poly(acrylamide-alginate) (AAm-Alg) gel [59]. The gel was synthesized by cross-linking photo-polymerization (1 h under UV light) of AAm monomers (12 wt.%) in an aqueous solution of Alg powder (2 wt.%) in the presence of calcium sulphate $CaSO_4 \cdot 2H_2O$ slurry (13.28 wt.% of Alg) as an ionic cross-linker for Alg, BIS (0.06 wt.% of AAm) as a covalent cross-linker for AAm, ammonium persulphate (APS) as an initiator, and TEMED (0.25 wt.% of AAm) as an accelerator. The double-network structure is formed by covalently cross-linked AAm chains (the first network) and ionically cross-linked Alg chains (the other network).

Tensile tests were conducted on as-prepared specimens with degree of swelling $Q_0 = 6.1$. The experimental program involves (i) loading–unloading tests with strain rate $\dot\epsilon = 0.033$ s^{-1} and various maximum elongation ratios $k_{\max}$ ranging from 4 to 13, and (ii) a multi-cycle test, in which a sample is stretched with strain rate $\dot\epsilon = 0.033$ s^{-1} up to elongation ratio $k_{\max\, 1} = 7$, unloaded down to the zero tensile stress, and reloaded up to elongation ratio $k_{\max\, 2} = 13$. Observations in the loading–unloading tests are depicted in Fig. 9 and those in the multi-cycle test are reported in Fig 10.

Matching experimental data in Fig. 9 is performed by means of the algorithm described in Sect.

3.2. Calculations show that each retraction path of the stress–strain diagrams in Fig. 9 is uniquely determined by the only parameter P_{1*} (R_1 remains independent of $k_{\max}$). Evolution of P_{1*} with maximum elongation ratio is illustrated in Fig. S9, where the data are approximated by Eq. (23). The best-fit material constants are collected in Tab. S6.

Keeping in mind that observations in Fig. 10 deviate slightly from those in Fig. 9, each set of data is approximated separately. Material constants determined by fitting observations along the first cycle of loading–retraction in Fig. 10 are listed in Tab. S6. The difference between the two sets of data in Tab. S6 is relatively small (for example, 7% for G and 11% for a), which confirms that the proposed algorithm for matching observations is stable.

We proceed with the analysis of observations on poly(N-isopropylacrylamide) (NIPA) gel reinforced with nanoclay (NC) Laponite XLG [54]. The gel was synthesized by photo-polymerization (2 h under UV light) of NIPA monomers (11 wt.%) in an aqueous dispersion of NC (5 wt.%) by using α-ketoglutaric acid (0.22 wt.%) as a photo-initiator. The double-network structure involves entangled NIPA chains connected to clay platelets by physical bonds (the first network) and exfoliated clay platelets bridged by electrostatic interaction (the other network).

Mechanical tests were conducted on as-prepared specimens with degree of swelling $Q_0 = 6.2$. The experimental program involves: (i) a series of loading-unloading tests with strain rate $\dot{\epsilon} = 0.01$ s^{-1} and maximum elongation ratios $k_{\max}$ ranging from 4 to 16, (ii) multi-cycle tests with the same strain rate, increasing maximum elongation ratios $k_{\max 1} = 4$, $k_{\max 2} = 8$, $k_{\max 3} = 12.5$ and minimum stress under retraction $\sigma_{\min} = 1$ kPa, and (iii) a multi-cycle test (3 cycles) with the strain rate $\dot{\epsilon}$, maximum elongation ratio $k_{\max} = 4$ and minimum stress $\sigma_{\min} = 1$ kPa.

Experimental data in the loading–unloading tests are depicted in Fig. 11, observations in the multi-cycle tests with increasing $k_{\max n}$ are reported in Fig 12, and those in the multi-cycle test with a fixed $k_{\max}$ are presented in Fig. 13. As experimental data under stretching do not coincide in these figures, each set of data is approximated separately by means of the algorithm suggested in Sect. 3.2. Adjustable parameters found by fitting observations are collected in Tab. S7.

Analysis of experimental data under retraction demonstrates that each unloading path in Figs. 10 to 12 is uniquely determined by the only parameter P_{1*} (R_1 is independent of $k_{\max}$). Changes in P_{1*} with $k_{\max}$ are illustrated in Fig. S10. The data are reported for all observations together with approximation of the corresponding dependence in Fig. 10 by Eq. (23).

Matching observations in Figs. 11 and 12 shows that each reloading path is uniquely determined by two parameters, P_{2*} and β_2 (R_2 is independent of deformation history). Changes in P_{2*} and

β_2 with $k_{\min}$ (the elongation ratio at the instant of transition from unloading to reloading) are demonstrated in Fig. S11, where the data are depicted together with their fit by Eq. (24).

Figs. S10 and S11 show that evolution of parameter P_{1*} with maximum elongation ratio per cycle $k_{\max}$ and evolution of parameters P_{2*} and β_2 with minimum elongation ratio per cycle $k_{\min}$ are practically independent of the deformation program.

To demonstrate the ability of the model to predict the response of DN gels under multi-cycle deformation, simulation is conducted of the governing equations with the material constants determined by matching observations in Fig 11B. Two deformation programs are considered: (i) with fixed maximum elongation ratio and the zero minimum stress, and (ii) with monotonically increasing elongation ratios under loading and the vanishing stress under retraction. Results of numerical analysis are reported in Figs. 14 and 15.

Stress–strain diagrams for multi-cycle (10 cycles) deformations with $k_{\max} = 4$ and 6 are presented in Fig. 14. This figure reveals that (i) the maximum stress per cycle $\sigma_{\max}$ decreases with number of cycles n, (ii) the minimum elongation ratio per cycle $k_{\min}$ increases with n, (iii) these parameters tend to their ultimate values with an increase in n, (iv) the rates of changes in $\sigma_{\max}$ and $k_{\min}$ with n grow with $k_{\max}$. These conclusions are in agreement with observations reported in [34, 35, 36].

Results of simulation for two multi-cycle programs (3 and 4 cycles) with monotonically increasing $k_{\max\, n}$ are reported in Fig. 15. This figure shows that (i) when elongation ratio k exceeds the maximum elongation ratio $k_{\max\, n}$ at the previous cycle of deformation, the stress–strain diagram under reloading reaches rapidly that under tension of a virgin sample (the Mullins effect), (ii) when the maximum elongation ratios coincide for two deformation programs, the corresponding retraction paths coincide as well (fading memory of deformation history). These results are in accord with experimental data presented in [37, 38, 39].

An advantage of our constitutive equations compared with the model developed in [41] (where observations on NIPA-NC gel were analyzed) consists in (i) the account for the time-dependent behavior and (ii) the ability to predict the response in multi-cycle tests with arbitrary elongation ratios at which the strain rate changes its sign.

The following conclusions are drawn:

(I) The model describes correctly multi-cycle deformation of DN gels (Figs. 10, 12, 13).

(II) Dissipative plastic flow under retraction and reloading is governed by Eqs. (23) and (24) (Figs. S10 and S11).

(III) The model provides reasonable predictions for the mechanical response in multi-cycle tests with one deformation program when its parameters are determined by fitting observations in experiments with another program (Figs. 14 and 15).

3.4 Damage accumulation under cyclic loading

In majority of experimental studies on DN gels subjected to multi-cycle tensile deformation, unloading of samples is conducted down to the zero strain (not zero stress). As a result, the stress–strain diagrams contain intervals with negative (compressive) stresses. Under compression, the samples are buckled [27], which leads to damage accumulation in the gels. Our purpose is to assess applicability of the model to the analysis of stress–strain curves on the damaged samples.

We study the mechanical response of poly(acrylamide–co-2-acrylamido-2-methyl propane sulfonic acid) (AAm–AMPS) gel reinforced with zirconium hydroxide $Zr(OH)_4$ nanoparticles (NP) [52]. The gel was prepared by free radical copolymerization (72 h at room temperature) of AAm and AMPS monomers (molar fraction of monomers 2 M, molar ratio 7:3) in colloidal solution (6 wt.%) of NP (average diameter 10 nm) by using KPS as an initiator (0.45 wt.% of monomers) and TEMED (3.6 μL per gram of monomers) as a catalyst. According to [52], the double-network structure is formed by entanglements between polymer chains (the first network) and hydrogen bonds between sulfonyl hydroxide groups of AMPS chains and hydroxyl groups on the surfaces on NP (the other network).

Mechanical tests were performed on fully swollen specimens with a non-specified degree of swelling. The experimental program involves: (i) a series of loading-unloading tests with strain rate $\dot{\epsilon} = 0.005$ s^{-1} and maximum elongation ratios $k_{\max}$ ranging from 2 to 4, and (ii) a multi-cycle test (5 cycles) with the same strain rate, maximum elongation ratio $k_{\max} = 4$ and unloading down to the zero strain.

Experimental data in the loading–unloading tests are depicted in Fig. 16, and those in the multi-cycle test are reported in Fig 17. Keeping in mind that the data along the first cycle of loading–retraction do not coincide, each set of observations is approximated separately. The adjustable parameter are listed in Tab. S8, which shows that discrepancies between their values are rather small.

Each unloading path in Fig. 16 is uniquely determined by two parameters, P_{1*} and R_1. Evolution of these quantities with $k_{\max}$ is illustrated in Fig. S12, where the data are reported together with their approximations by Eq. (23). Fitting of observations in Fig. 17 shows that parameters

P_{1*} and R_1 (that characterize each retraction path in this figure) remain independent of n. Their values are reported in Tab. S8.

Each set of observations along reloading paths in Fig. 17 is approximated separately. In the fitting procedure, we suppose that unloading occurs down to the stress $\sigma_{\min} = -0.03$ MPa (this value is chosen from the best-fit condition) and disregard buckling of samples under compression. The quantities P_{2*} and R_2 are found by matching the first reloading path ($n = 2$). After fixing their values, the other paths are approximated with the help of the only parameter β_2. The dependence of this quantity on number of cycles n is illustrated in Fig. S13. The data are approximated by the equation

$$\log \beta_2 = \beta_2^0 - \beta_2^1 n, \tag{25}$$

where the coefficients are determined by the least-squares method.

It is worth noting that the values of P_{2*}, R_2 and β_2 under reloading have the same order of magnitude for all materials under consideration: $P_{2*} = 2.3 \cdot 10^{-8}$ for AAm-Alg gel, $7.0 \cdot 10^{-8}$ for AAm–AMPS–NP gel, and from $9.0 \cdot 10^{-8}$ to $2.3 \cdot 10^{-7}$ s^{-1} for NIPA-NC gel; $R_2 = 1.2 \cdot 10^3$ for AAm–AMPS–NP gel, from $2.9 \cdot 10^3$ to $4.5 \cdot 10^3$ for NIPA-NC gel, and $1.2 \cdot 10^4$ for AAm-Alg gel; $\beta_2 = 19$ for AAm–AMPS–NP gel, 52 for AAm-Alg gel, and from 59 to 119 MPa^{-1} for NIPA-NC gel.

To demonstrate the ability of the model to predict observations, numerical analysis is performed of the mechanical behavior of AAm–AMPS–NP gel under multi-cycle (20 cycles) deformation with $k_{\max} = 4$ and $\sigma_{\min} = 0$. Results of simulation are depicted in Fig. 18. Fig. 18A shows the entire stress–strain diagram, and Fig. 18B demonstrates the decay in maximum stress per cycle $\sigma_{\max}$ with number of cycles n. The latter dependence is in accord with observations reported in [73, 74].

The following conclusions are drawn:

(I) The model can be applied to the analysis of observations on DN gels subjected to multi-cycle deformation accompanied by buckling-induced damage (Fig. 17).

(II) Eq. (25) provides a simple way to account for damage accumulation induced by buckling of samples under compression (Fig. S13).

(III) The approach grounded on Eq. (25) leads to reasonable predictions of the response in multi-cycle tests (Fig. 18).

Approximation of observations in mechanical tests implies that $\kappa < 1$ for all DN gels under consideration (Tabs. S1 to S8). This means that some junctions between chains are treated as permanent even when the gels are synthesized without covalent cross-links. This is not surprising

for two reasons: (i) the rate of reptation of chains is strongly reduced due to the presence of temporary bonds, which implies that some entanglements remain ineradicable, and (ii) to avoid evaporation of water from hydrogels, the duration of mechanical tests does not exceed a few minutes, which means that physical junctions whose characteristic time for rearrangement exceed this time should be considered as permanent.

4 Concluding remarks

A constitutive model is developed for the viscoelastic and viscoplastic behavior of DN gels with covalent and non-covalent bonds. The equivalent polymer network in a gel is treated as a combination of two networks: chains in the first network are linked by permanent junctions, while chains in the other network are bridged by temporary bonds.

The viscoelastic response of a gel reflects breakage and reformation of temporary junctions in the transient network (transition of chains connected by physical bonds from their active to dangling state and vice versa). To describe observations in relaxation tests and tensile tests with various strain rates, the transient network is presumed to be inhomogeneous and composed of meso-regions with different rates for rearrangement of junctions. This approach allows the entire relaxation spectrum to be accounted for in terms of a distribution function for meso-regions with various activation energies for breakage of temporary bonds.

The viscoplastic behavior of a gel reflects slippage of junctions in the permanent network with respect to their reference positions. Motion of a junction starts when the junction becomes unbalanced due to transformation of one of the chains connected by this junction from its active state into the dangling state (which means that stress in this chain vanishes suddenly). The junction proceeds to slide with respect to the network (plastic flow) until it reaches a new equilibrium state.

The characteristic feature of the model is the presence of two mechanisms for plastic deformation: (i) non-dissipative, when junctions slide with respect to their initial positions with the rate proportional to the strain rate, and (ii) dissipative with the rate of sliding determined by the energy of inter-chain interaction. The kinetics of dissipative plastic flow under cyclic deformation is governed by differential equations with coefficients adopting different values under the first loading, retraction and reloading.

The model is applied to approximate experimental data in tensile tests with various strain rates, relaxation tests, loading-unloading tests, and multi-cycle tests with two deformation programs on

a series of DN gels with covalent and non-covalent bonds. Numerical simulation demonstrates that (i) experimental stress–strain diagrams are described adequately by the governing equations, (ii) material parameters evolve consistently with experimental conditions (maximum elongation ratio under stretching and minimum elongation ratio under retraction), and (iii) predictions of the model are in quantitative (where sufficient data are provided) and qualitative agreement with observations.

Although the model can be employed for the analysis of the mechanical behavior of DN gels under arbitrary three-dimensional deformations, this paper focuses on observations in tensile tests with strain-controlled programs and relatively small number of cycles. We believe that after an appropriate modifications, the model can be applied for the analysis (i) of the viscoelastic and viscoplastic responses of these gels under multiaxial deformation, (ii) the kinetics of their self-healing and self-recovery [75], as well as (iii) for the assessment of their life-time under fatigue conditions [76].

Acknowledgments

Financial support by the Danish Innovation Fund (project 5152-00002B) is gratefully acknowledged.

References

[1] M.A. Haque, T. Kurokawa, J.P. Gong, Super tough double network hydrogels and their application as biomaterials. Polymer 53 (2012) 1805–1822.

[2] N. Annabi, A. Tamayol, J.A. Uquillas, M. Akbari, L.E. Bertassoni, C. Cha, G. Camci-Unal, M.R. Dokmeci, N.A. Peppas, A. Khademhosseini, Rational design and applications of hydrogels in regenerative medicine. Adv. Mater. 26 (2014) 85–124.

[3] Y. Jiang, J. Chen, C. Deng, E.J. Suuronen, Z. Zhong, Click hydrogels, microgels and nanogels: Emerging platforms for drug delivery and tissue engineering. Biomaterials 35 (2014) 4969–4985.

[4] N.A. Peppas, D.S. Van Blarcom, Hydrogel-based biosensors and sensing devices for drug delivery. J. Control. Release 240 (2016) 142–150.

[5] Y. Shi, J. Zhang, L. Pan, Y. Shi, G. Yu, Energy gels: A bio-inspired material platform for advanced energy applications. Nano Today 11 (2016) 738–762.

[6] L. An, T.S. Zhao, L. Zeng, Agar chemical hydrogel electrode binder for fuel-electrolyte-fed fuel cells. Appl. Energy 109 (2013) 67–71.

[7] L. An, R. Chen, Mathematical modeling of direct formate fuel cells. Appl. Therm. Eng. 124 (2017) 232–240.

[8] Z.F. Pan, L. An, T.S. Zhao, Z.K. Tang, Advances and challenges in alkaline anion exchange membrane fuel cells. Prog. Energy Combust. Sci. 66 (2018) 141–175.

[9] J. Bae, Y. Li, J. Zhang, X. Zhou, F. Zhao, Y. Shi, J.B. Goodenough, G. Yu, A 3D nanostructured hydrogel-framework-derived high-performance composite polymer Lithium-ion electrolyte. Angew. Chem. Int. Ed. 57 (2018) 2096–2100.

[10] P. Li, Z. Jin, L. Peng, F. Zhao, D. Xiao, Y. Jin, G. Yu, Stretchable all-gel-state fiber-shaped supercapacitors enabled by macromolecularly interconnected 3D graphene/nanostructured conductive polymer hydrogels. Adv. Mater. 30 (2018) 1800124.

[11] Y. Tanaka, R. Kuwabara, Y.-H. Na, T. Kurokawa, J.P. Gong, Y. Osada, Determination of fracture energy of high strength double network hydrogels. J. Phys. Chem. B 109 (2005) 11559–11562.

[12] J.P. Gong, Materials both tough and soft. Science 344 (2014) 161–162.

[13] R.J. Wojtecki, M.A. Meador, S.J. Rowan, Using the dynamic bond to access macroscopically responsive structurally dynamic polymers. Nat. Mater. 10 (2011) 14–27.

[14] X. Zhao, Multi-scale multi-mechanism design of tough hydrogels: Building dissipation into stretchy networks. Soft Matter 10 (2014) 672–687.

[15] A. Vedadghavami, F. Minooei, M.H. Mohammadi, S. Khetani, A.R. Kolahchi, S. Mashayekhan, A. Sanati-Nezhad, Manufacturing of hydrogel biomaterials with controlled mechanical properties for tissue engineering applications. Acta Biomater. 62 (2017) 42–63.

[16] Q. Chen, H. Chen, L. Zhu, J. Zheng, Engineering of tough double network hydrogels. Macromol. Chem. Phys. 217 (2016) 1022–1036.

[17] C. Creton, Networks and gels: Soft but dynamic and tough. Macromolecules 50 (2017) 8297–8316.

[18] W. Wang, Y. Zhang, W. Liu, Bioinspired fabrication of high strength hydrogels from non-covalent interactions. Progr. Polym. Sci. 71 (2017) 1–25.

[19] T. Beda, An approach for hyperelastic model-building and parameters estimation: a review of constitutive models. Eur. Polym. J. 50 (2014) 97–108.

[20] S. Rose, A. Dizeux, T. Narita, D. Hourdet, A. Marcellan, Time dependence of dissipative and recovery processes in nanohybrid hydrogels. Macromolecules 46 (2013) 4095–4104.

[21] S.C. Grindy, R. Learsch, D. Mozhdehi, J. Cheng, D.G. Barrett, Z. Guan, P.B. Messersmith, N. Holten-Andersen, Control of hierarchical polymer mechanics with bioinspired metal-coordination dynamics. Nat. Mater. 14 (2015) 1210–1217.

[22] F. Meng, R.H. Pritchard, E.M. Terentjev, Stress relaxation, dynamics, and plasticity of transient polymer networks. Macromolecules 49 (2016) 2843–2852.

[23] X. Hu, J. Zhou, W.F.M. Daniel, M. Vatankhah-Varnoosfaderani, A.V. Dobrynin, S.S. Sheiko, Dynamics of dual networks: Strain rate and temperature effects in hydrogels with reversible H-bonds. Macromolecules 50 (2017) 652–659.

[24] M.S. Green, A.V. Tobolsky, A new approach to the theory of relaxing polymeric media. J. Chem. Phys. 14 (1946) 80–92.

[25] F. Tanaka, S.F. Edwards, Viscoelastic properties of physically cross-linked networks. Transient network theory. Macromolecules 25 (1992) 1516–1523.

[26] K.N. Long, The mechanics of network polymers with thermally reversible linkages. J. Mech. Phys. Solids 63 (2014) 386–411.

[27] R. Long, K. Mayumi, C. Creton, T. Narita, C.Y. Hui, Time dependent behavior of a dual cross-link self-healing gel: theory and experiments. Macromolecules 47 (2014) 7243–7250.

[28] A.D. Drozdov, P. Sommer-Larsen, J. deClaville Christiansen, C.-G. Sanporean, Time-dependent response of hydrogels under constrained swelling. J. Appl. Phys. 115 (2014) 233517.

[29] J. Guo, R. Long, K. Mayumi, C.-Y. Hui, Mechanics of a dual cross-link gel with dynamic bonds: Steady state kinetics and large deformation effects. Macromolecules 49 (2016) 3497–3507.

[30] Q. Wang, Z. Gao, A constitutive model of nanocomposite hydrogels with nanoparticle crosslinkers. J. Mech. Phys. Solids 94 (2016) 127–147.

[31] F.J. Vernerey, R. Long, R. Brighenti, A statistically-based continuum theory for polymers with transient networks. J. Mech. Phys. Solids 107 (2017) 1–20.

[32] A.D. Drozdov, Modeling the response of double-network gels with sacrificial junctions under swelling. Int. J. Solids Struct. 122–123 (2017) 175–188.

[33] Y. Mao, S. Lin, X. Zhao, L. Anand, A large deformation viscoelastic model for double-network hydrogels. J. Mech. Phys. Solids 100 (2017) 103–130.

[34] P. Lin, S. Ma, X. Wang, F. Zhou, Molecularly engineered dual-crosslinked hydrogel with ultrahigh mechanical strength, toughness, and good self-recovery. Adv. Mater. 27 (2015) 2054–2059.

[35] X. Liang, Y. Deng, X. Pei, K. Zhai, K. Xu, Y. Tan, X. Gong, P. Wang, Tough, rapid-recovery composite hydrogels fabricated via synergistic coreshell microgel covalent bonding and Fe^{3+} coordination cross-linking. Soft Matter 13 (2017) 2654–2662.

[36] C. Shao, H. Chang, M. Wang, F. Xu, J. Yang, High-strength, tough, and self-healing nanocomposite physical hydrogels based on the synergistic effects of dynamic hydrogen bond and dual coordination bonds. ACS Appl. Mater. Interfaces 9 (2017) 28305–28318.

[37] Q. Chen, X. Yan, L. Zhu, H. Chen, B. Jiang, D. Wei, L. Huang, J. Yang, B. Liu, J. Zheng, Improvement of mechanical strength and fatigue resistance of double network hydrogels by ionic coordination interactions. Chem. Mater. 28 (2016) 5710–5720.

[38] X. Li, Q. Yang, Y. Zhao, S. Long, J. Zheng, Dual physically crosslinked double network hydrogels with high toughness and self-healing properties. Soft Matter 13 (2017) 911–920.

[39] H. Huang, Y. Wang, X. Wang, F. Rehfeldt, K. Zhang, Robust heterogeneous hydrogels with dynamic nanocrystal–polymer interface. Macromol. Rapid Commun. 38 (2017) 1600810.

[40] X. Zhao, A theory for large deformation and damage of interpenetrating polymer networks. J. Mech. Phys. Solids 60 (2012) 319–332.

[41] J. Tang, X. Chen, Y. Pei, D. Fang, Pseudoelasticity and nonideal Mullins effect of nanocomposite hydrogels. J. Appl. Mech. 83 (2016) 111010.

[42] T. Lu, J. Wang, R. Yang, T.J. Wang, A constitutive model for soft materials incorporating viscoelasticity and Mullins effect. J. Appl. Mech. 84 (2017) 021010.

[43] A.D. Drozdov, J. deClaville Christiansen, Nanocomposite gels with permanent and transient junctions under cyclic loading. Macromolecules 51 (2018) 1462–1473.

[44] A. Perez-San Vicente, M. Peroglio, M. Ernst, P. Casuso, I. Loinaz, H.-J. Grande, M. Alini, D. Eglin, D. Dupin, Self-healing dynamic hydrogel as injectable shock-absorbing artificial nucleus pulposus. Biomacromolecules 18 (2017) 2360–2370.

[45] F. Yang, V. Tadepalli, B.J. Wiley, 3D printing of a double network hydrogel with a compression strength and elastic modulus greater than those of cartilage. ACS Biomater. Sci. Eng. 3 (2017) 863–869.

[46] M. Bohdan, J. Sprakel, J. van der Gucht, Multiple relaxation modes in associative polymer networks with varying connectivity. Phys. Rev. E 94 (2016) 032507.

[47] A.D. Drozdov, R.K. Gupta, Non-linear viscoelasticity and viscoplasticity of isotactic polypropylene. Int. J. Eng. Sci. 41 (2003) 2335–2361.

[48] A.D. Drozdov, Creep rupture and viscoelastoplasticity of polypropylene. Eng. Fract. Mech. 77 (2010) 2277–2293.

[49] E. Filippidi, T.R. Cristiani, C.D. Eisenbach, J.H. Waite, J.N. Israelachvili, B.K. Ahn, M.T. Valentine, Toughening elastomers using mussel-inspired iron-catechol complexes. Science 358 (2017) 502–505.

[50] K. Mayumi, A. Marcellan, G. Ducouret, C. Creton, T. Narita, Stress–strain relationship of highly stretchable dual cross-link gels: Separability of strain and time effect. ACS Macro Lett. 2 (2013) 1065–1068.

[51] L. Carlsson, S. Rose, D. Hourdet, A. Marcellan, Nano-hybrid self-crosslinked PDMA/silica hydrogels. Soft Matter 6 (2010) 3619–3631.

[52] H. Jiang, G. Zhang, X. Feng, H. Liu, F. Li, M. Wang, H. Li, Room-temperature self-healing tough nanocomposite hydrogel crosslinked by zirconium hydroxide nanoparticles. Compos. Sci. Technol. 140 (2017) 54–62.

[53] A. Klein, P.G. Whitten, K. Resch, G. Pinter, Nanocomposite hydrogels: Fracture toughness and energy dissipation mechanisms. J. Polym. Sci., Part B: Polym. Phys. 53 (2015) 1763–1773.

[54] J. Tang, G. Xu, Y. Sun, Y. Pei, D. Fang, Dissipative properties and chain evolution of highly strained nanocomposite hydrogel. J. Appl. Phys. 116 (2014) 244901.

[55] K. Peng, H. Yu, H. Yang, X. Hao, A. Yasin, X. Zhang, A mechanically robust hydrogel with thermally induced plasticity and a shape memory effect. Soft Matter 13 (2017) 2135–2140.

[56] Z. Qin, R. Niu, C. Tang, J. Xia, F. Ji, D. Dong, H. Zhang, S. Zhang, J. Li, F. Yao, A dual-crosslinked strategy to construct physical hydrogels with high strength, toughness, good mechanical recoverability, and shape-memory ability. Macromol. Mater. Eng. 303 (2018) 1700396.

[57] M.A. Haque, T. Kurokawa, G. Kamita, J.P. Gong, Lamellar bilayers as reversible sacrificial bonds to toughen hydrogel: Hysteresis, self-recovery, fatigue resistance, and crack blunting. Macromolecules 44 (2011) 8916–8924.

[58] X. Li, T. Kurokawa, R. Takahashi, M.A. Haque, Y. Yue, T. Nakajima, J.P. Gong, Polymer adsorbed bilayer membranes form self-healing hydrogels with tunable superstructure. Macromolecules 48 (2015) 2277–2282.

[59] J.-Y. Sun, X. Zhao, W.R.K. Illeperuma, O. Chaudhuri, K.H. Oh, D.J. Mooney, J.J. Vlassak, Z. Suo, Highly stretchable and tough hydrogels. Nature 489 (2012) 133–136.

[60] A.D. Drozdov, R. Klitkou, J.deC. Christiansen, Cyclic viscoplasticity of semicrystalline polymers with finite deformations. Mech. Mater. 56 (2013) 53–64.

[61] A.D. Drozdov, R.K. Gupta, Constitutive equations in finite viscoplasticity of semicrystalline polymers. Int. J. Solids Struct. 40 (2003) 6217–6243.

[62] A.D. Drozdov, Cyclic thermo-viscoplasticity of high density polyethylene. Int. J. Solids Struct. 47 (2010) 1592–1602.

[63] K. Cui, T.L. Sun, T. Kurokawa, T. Nakajima, T. Nonoyama, L. Chen, J.P. Gong, Stretching-induced ion complexation in physical polyampholyte hydrogels. Soft Matter 12 (2016) 8833–8840.

[64] A.D. Drozdov, Self-oscillations of hydrogels driven by chemical reactions. Int. J. Appl. Mech. 6 (2014) 1450023.

[65] A.N. Gent, A new constitutive relation for rubber. Rubber Chem. Technol. 69 (1996) 59–61.

[66] T. Narita, K. Mayumi, G. Ducouret, P. Hebraud, Viscoelastic properties of poly(vinyl alcohol) hydrogels having permanent and transient cross-links studied by microrheology, classical rheometry, and dynamic light ccattering. Macromolecules 46 (2013) 4174–4183.

[67] M. Shibayama, M. Sato, Y. Kimura, H. Fujiwara, S. Nomura, ^{11}B n.m.r, study on the reaction of poly(vinyl alcohol) with boric acid. Polymer 29 (1988) 336–340.

[68] C.R. Lopez-Barron, R. Chen, N.J. Wagner, Ultrastretchable iono-elastomers with mechano-electrical response. ACS Macro Lett. 5 (2016) 1332–1338.

[69] X. Hu, J. Zhou, W.F.M. Daniel, M. Vatankhah-Varnoosfaderani, A.V. Dobrynin, S.S. Sheiko, Dynamics of dual networks: Strain rate and temperature effects in hydrogels with reversible H-bonds. Macromolecules 50 (2017) 652–659.

[70] Q. Chen, D. Wei, H. Chen, L. Zhu, C. Jiao, G. Liu, L. Huang, J. Yang, L. Wang, J. Zheng, Simultaneous enhancement of stiffness and toughness in hybrid double-network hydrogels via the first, physically linked network. Macromolecules 48 (2015) 8003–8010.

[71] F. Luo, T.L. Sun, T. Nakajima, T. Kurokawa, Y. Zhao, K. Sato, A.B. Ihsan, X. Li, H. Guo, J.P. Gong, Oppositely charged polyelectrolytes form tough, self-healing, and rebuildable hydrogels. Adv. Mater. 27 (2015) 2722–2727.

[72] F. Zhu, X.Y. Lin, Z.L. Wu, L. Cheng, J. Yin, Y. Song, J. Qian, Q. Zheng, Processing tough supramolecular hydrogels with tunable strength of polyion complex. Polymer 95 (2016) 9–17.

[73] L. Zhang, J. Zhao, J. Zhu, C. Hea, H. Wang, Anisotropic tough poly(vinyl alcohol) hydrogels. Soft Matter 8 (2012) 10439–10447.

[74] P. Wang, G. Deng, L. Zhou, Z. Li, Y. Chen, Ultrastretchable, self-healable hydrogels based on dynamic covalent bonding and triblock copolymer micellization. ACS Macro Lett. 6 (2017) 881–886.

[75] T.L. Sun, K. Cui, J.P. Gong, Tough, self-recovery and self-healing polyampholyte hydrogels. Polym. Sci. C 59 (2017) 11–17.

[76] W. Zhang, X. Liu, J. Wang, J. Tang, J. Hu, T. Lu, Z. Suo, Fatigue of double-network hydrogels. Eng. Fracture Mech. 187 (2018) 74–93.

List of figures

Figure 1: A: Tensile stress σ versus relaxation time $t_{\rm rel}$. Circles: experimental data [27] in relaxation test with $k_{\max} = 1.1$ and strain rate under loading $\dot{\epsilon} = 0.2$ s^{-1}. Solid line: results of simulation. B: Tensile stress σ versus elongation ratio k. Symbols: experimental data [27] in tensile tests with various strain rates $\dot{\epsilon}$ s^{-1}. Solid lines: results of simulation.

Figure 2: Tensile stress σ versus elongation ratio k. Symbols: experimental data [27] in cyclic tests with $k_{\max} = 1.3$, strain rates under loading $\dot{\epsilon}_1 = 0.01$ s^{-1} (A) and $\dot{\epsilon}_1 = 0.3$ s^{-1} (B), and various strain rates under retraction $\dot{\epsilon}_2$ s^{-1}. Solid lines: Predictions of the model.

Figure 3: A: Tensile stress σ versus elongation ratio k. Circles: experimental data [51] on DMA-NP gel in cyclic test with strain rate $\dot{\epsilon} = 0.06$ s^{-1} and maximum elongation ratio $k_{\max} = 6$. Solid line: results of simulation. B: Ratio of tensile stresses $S = \sigma(t_{\rm rel})/\sigma(0)$ versus relaxation time $t_{\rm rel}$. Circles: experimental data [51] on DMA-NP gel in relaxation test with $k_{\max} = 1.5$ and strain rate under stretching $\dot{\epsilon} = 0.06$ s^{-1}. Solid line: results of simulation.

Figure 4: A: Tensile stress σ versus elongation ratio k. Circles: experimental data [53] on DMA-NC gel in cyclic test with strain rate $\dot{\epsilon} = 0.005$ s^{-1} and maximum elongation ratio $k_{\max} = 6$. Solid line: results of simulation. B: Tensile stress σ versus relaxation time $t_{\rm rel}$. Circles: experimental data [53] on DMA-NC gel in relaxation test with $k_{\max} = 2$ and strain rate under stretching $\dot{\epsilon} = 0.5$ s^{-1}. Solid line: results of simulation.

Figure 5: Tensile stress σ versus elongation ratio k. Symbols: experimental data [55] on AAm–AAc–ODA gel in cyclic tests with strain rate $\dot{\epsilon} = 0.083$ s^{-1} and various maximum elongation ratios $k_{\max}$. Solid lines: results of simulation.

Figure 6: Tensile stress σ versus elongation ratio k. Symbols: experimental data [56] in cyclic tests on AAm–AAc–SMA gel with strain rate $\dot{\epsilon} = 0.167$ s^{-1} and various maximum elongation ratios $k_{\max}$. Solid lines: results of simulation.

Figure 7: Tensile stress σ versus elongation ratio k. Symbols: experimental data [57] in cyclic tests on AAm–DGI gel (0.13 M of DGI) with strain rate $\dot{\epsilon} = 0.005$ s^{-1} and various maximum elongation ratios $k_{\max}$. Solid lines: results of simulation.

Figure 8: Tensile stress σ versus elongation ratio k. Circles: experimental data [57] in cyclic test on AAm–DGI gel (0.1 M of DGI) with strain rate $\dot{\epsilon} = 0.005$ s^{-1} and maximum elongation

ratio $k_{\max} = 5$. Solid line: results of simulation.

Figure 9: Tensile stress σ versus elongation ratio k. Symbols: experimental data [59] on AAm-alginate gel in cyclic tests with strain rate $\dot{\epsilon} = 0.033$ s^{-1} and various maximum elongation ratios $k_{\max}$. Solid lines: results of simulation.

Figure 10: Tensile stress σ versus elongation ratio k. Symbols: experimental data [59] on AAm-alginate gel in multi-cycle test with strain rate $\dot{\epsilon} = 0.033$ s^{-1} and maximum elongation ratios $k_{\max 1} = 7$, $k_{\max 2} = 13$. Dotted line: results of simulation for tensile test. Solid line: results of simulation for multi-cycle test.

Figure 11: Tensile stress σ versus elongation ratio k. Symbols: experimental data [54] in cyclic tests on NIPA-NC gel with strain rate $\dot{\epsilon} = 0.01$ s^{-1} and various maximum elongation ratios $k_{\max}$. Solid lines: results of simulation.

Figure 12: Tensile stress σ versus elongation ratio k. A: Symbols: experimental data [54] in cyclic test on NIPA-NC gel with $\dot{\epsilon} = 0.01$ s^{-1}, $k_{\max 1} = 4$, $k_{\max 2} = 8$ and $\sigma_{\min} = 1.4$ kPa. Dotted line: results of simulation for tensile test. Solid line: results of simulation for the multi-cycle test. B: Symbols: experimental data [54] in cyclic with $\dot{\epsilon} = 0.01$ s^{-1}, $k_{\max 1} = 4.2$, $k_{\max 2} = 8.2$, $k_{\max 3} = 12.5$. Dotted line: results of simulation for one-cycle test with $k_{\max} = 12.5$. Solid line: results of simulation for the multi-cycle test.

Figure 13: Tensile stress σ versus elongation ratio k. Symbols: experimental data [54] on NIPA-NC gel in multi-cycle test with $n = 3$, $\dot{\epsilon} = 0.01$ s^{-1}, $k_{\max} = 4$ and $\sigma_{\min} = 1.0$ kPa. Solid line: results of simulation.

Figure 14: Tensile stress σ versus elongation ratio k. Solid lines: results of numerical simulation for multi-cycle tests on NIPA-NC gel with $n = 10$, $\dot{\epsilon} = 0.01$ s^{-1} and $\sigma_{\min} = 0$. A: $k_{\max} = 4$. B: $k_{\max} = 6$.

Figure 15: Tensile stress σ versus elongation ratio k. Solid lines: results of numerical simulation for multi-cycle tests on NIPA-NC gel with $\dot{\epsilon} = 0.01$ s^{-1} and $\sigma_{\min} = 0$. A: $n = 3$, $k_{\max 1} = 5$, $k_{\max 2} = 9$, $k_{\max 3} = 13$. B: $n = 4$, $k_{\max 1} = 4$, $k_{\max 2} = 7$, $k_{\max 3} = 10$, $k_{\max 4} = 13$.

Figure 16: Tensile stress σ versus elongation ratio k. Symbols: experimental data [52] in cyclic tests on AAm–AMPS–NP gel with strain rate $\dot{\epsilon} = 0.005$ s^{-1} and various maximum elongation ratios $k_{\max}$. Solid lines: results of simulation.

Figure 17: Tensile stress σ versus elongation ratio k. Symbols: experimental data [52] on AAm–AMPS–NP gel in multi-cycle test with $n = 5$, $\dot{\epsilon} = 0.005\ \mathrm{s}^{-1}$, $\sigma_{\min} = -0.03$ MPa and $k_{\max} = 4$. Solid lines: results of simulation.

Figure 18: A: Tensile stress σ versus elongation ratio k. B: Maximum stress per cycle $\sigma_{\max}$ versus number of cycles n. Solid line and circles: results of simulation for multi-cycle test on AAm–AMPS–NP gel with $n = 20$, $\dot{\epsilon} = 0.005\ \mathrm{s}^{-1}$, $\sigma_{\min} = 0$ and $k_{\max} = 4$.

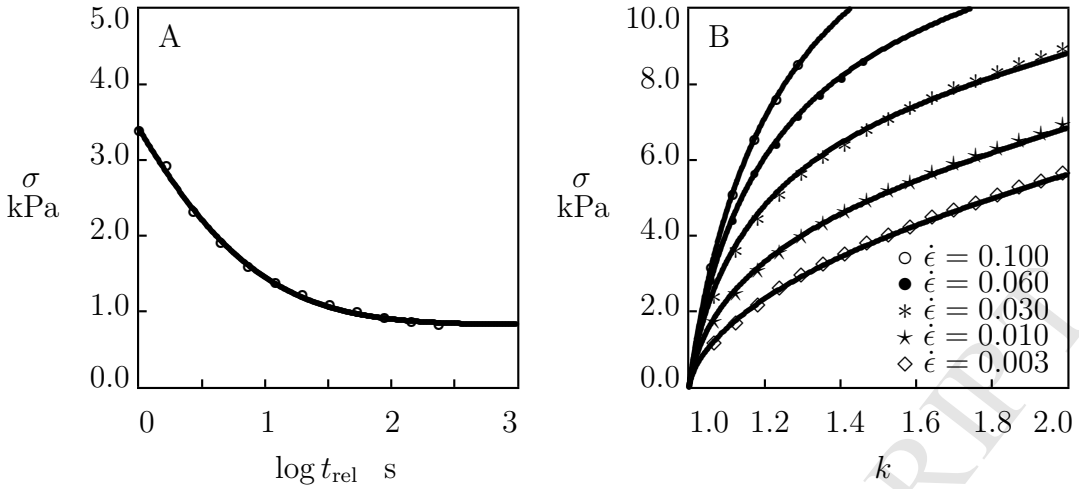

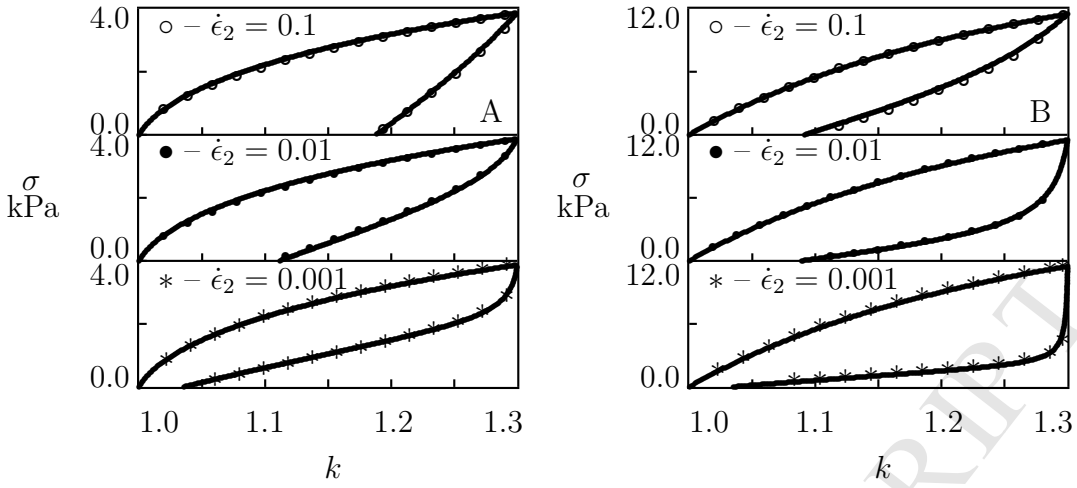

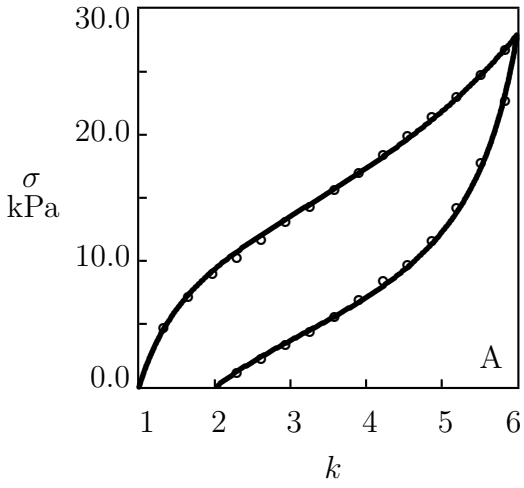

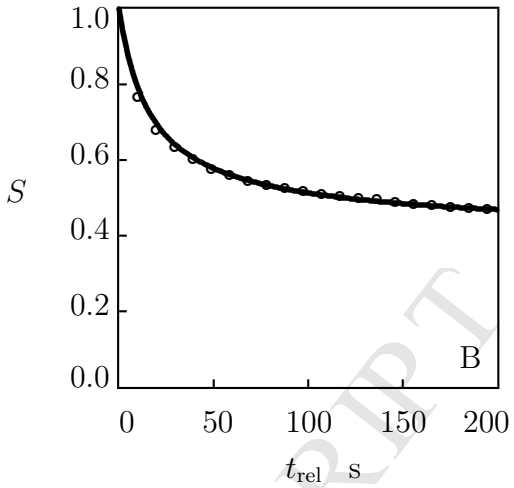

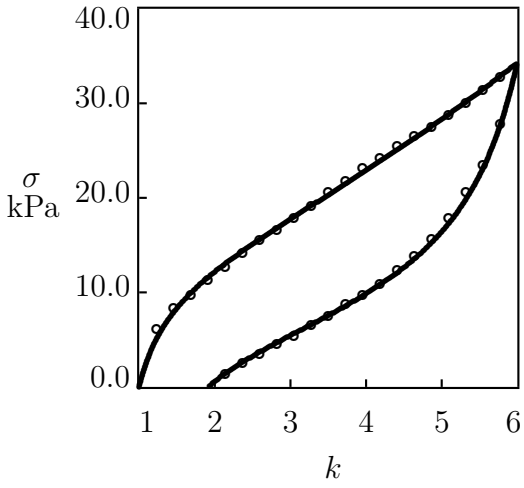

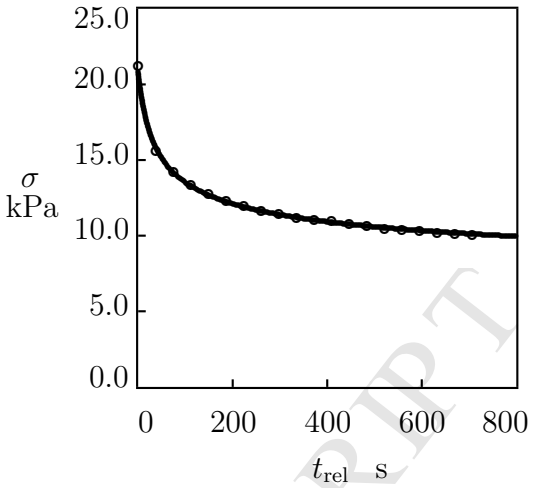

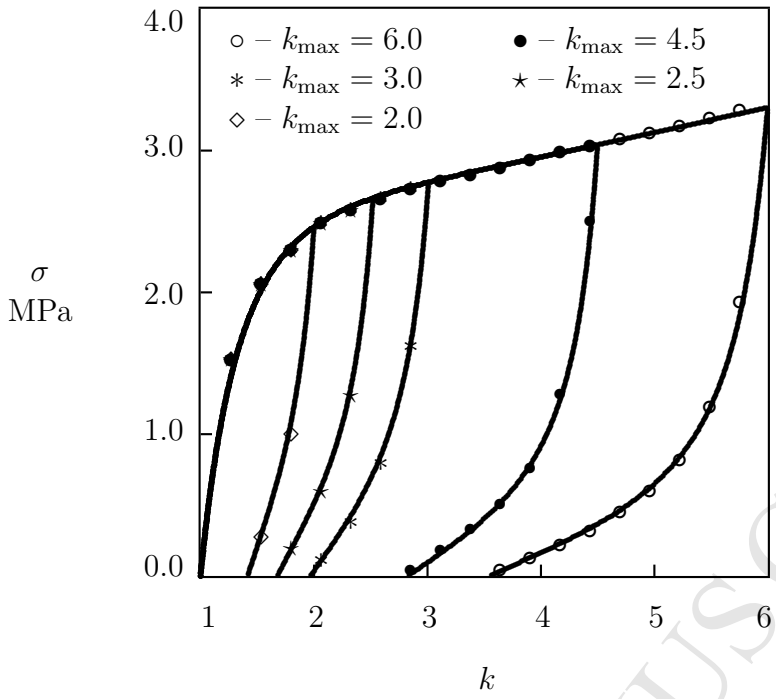

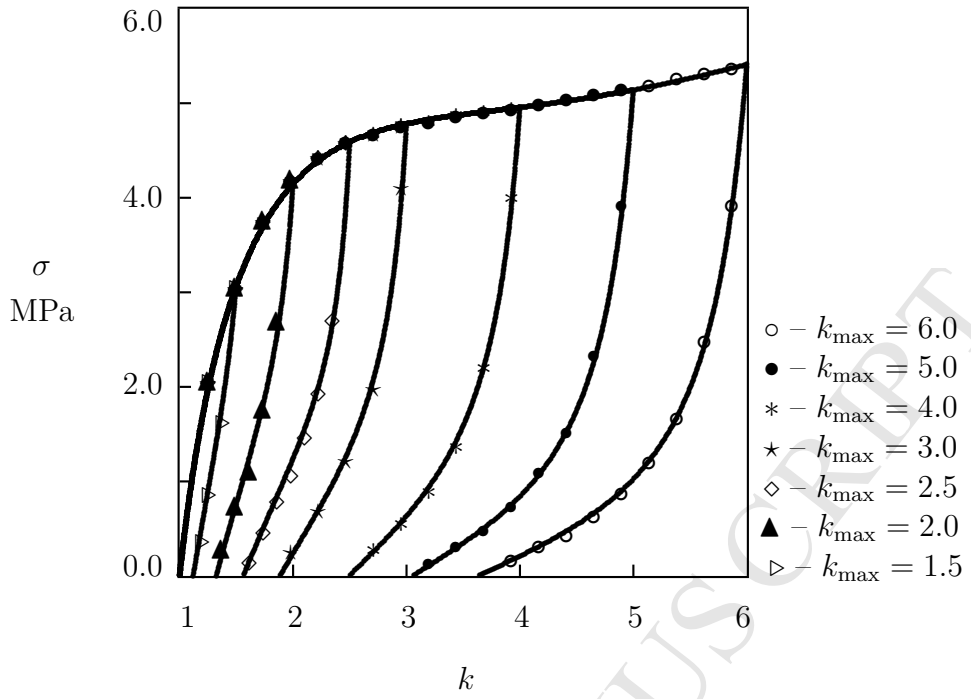

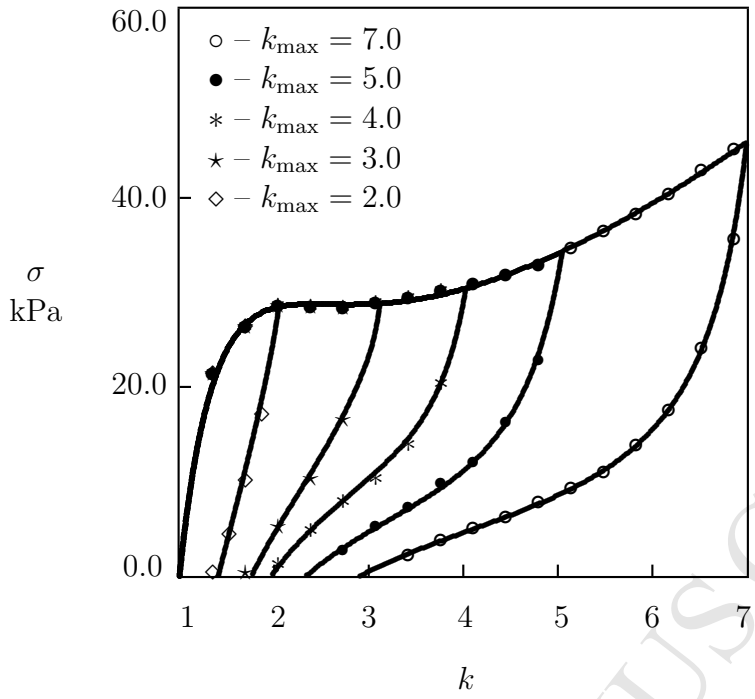

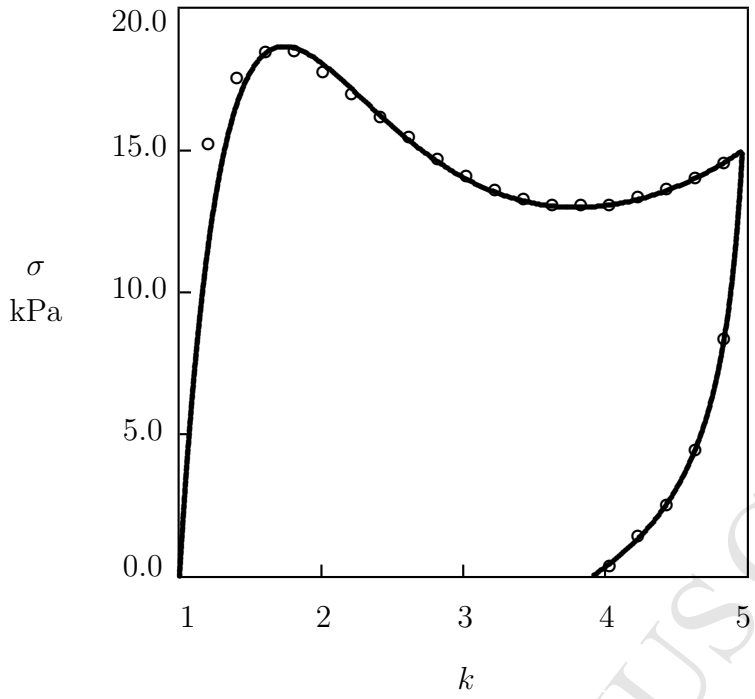

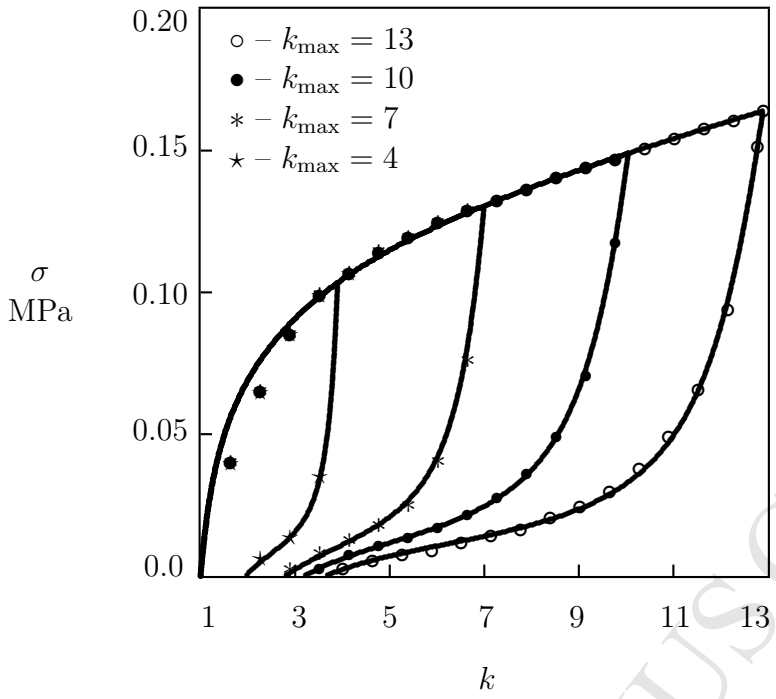

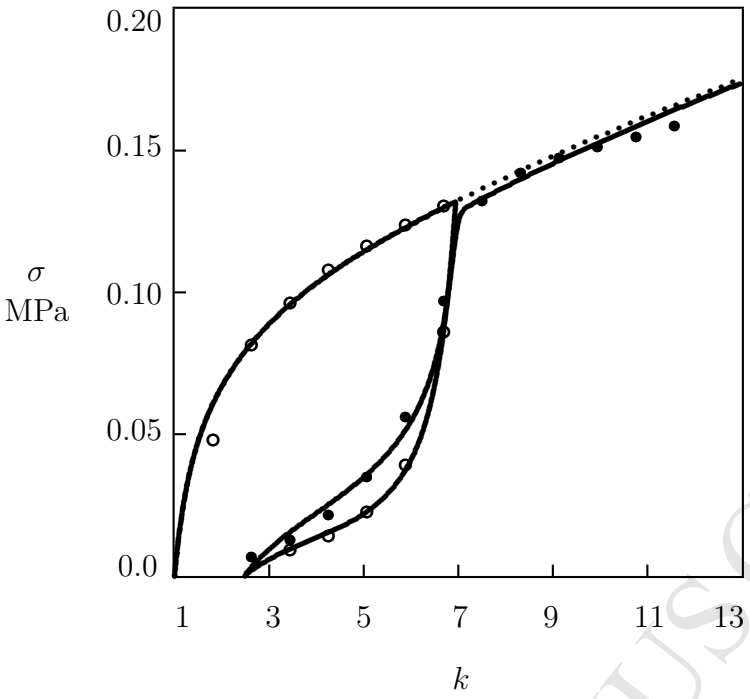

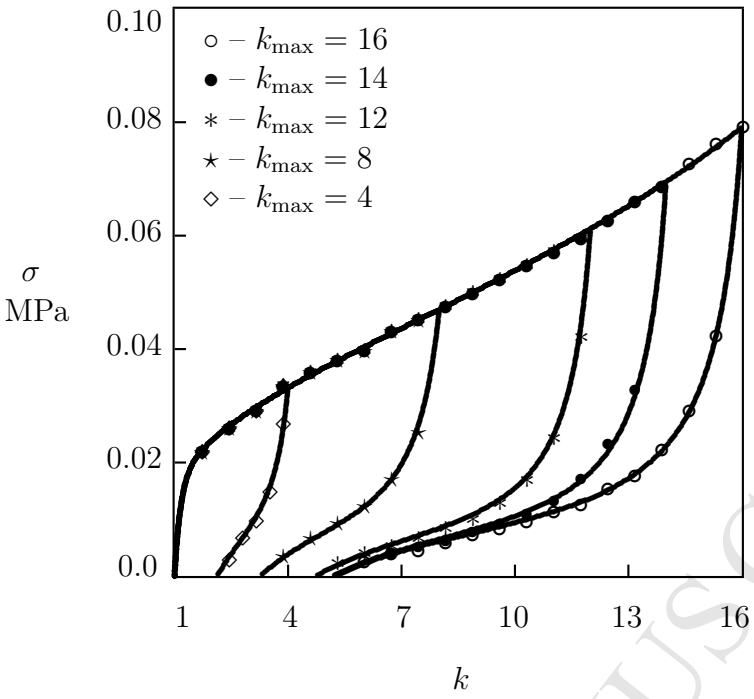

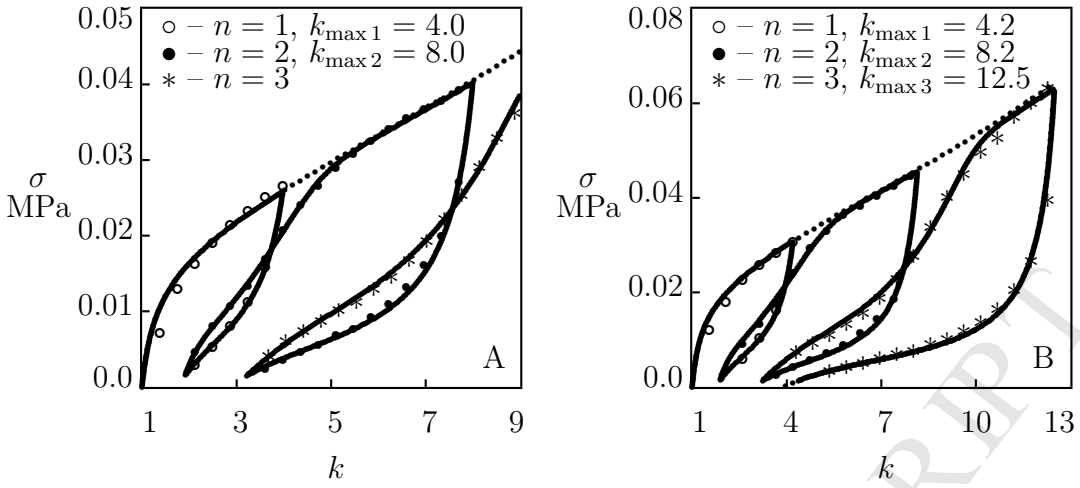

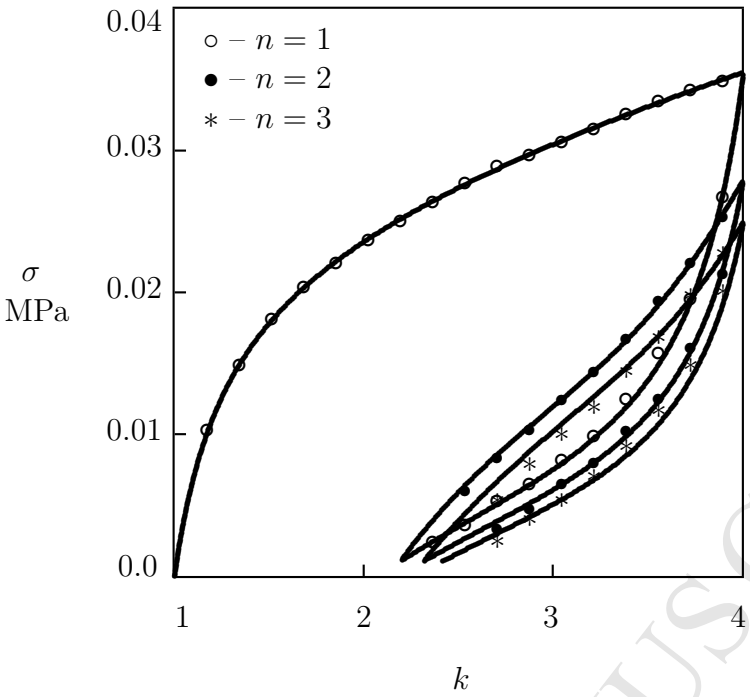

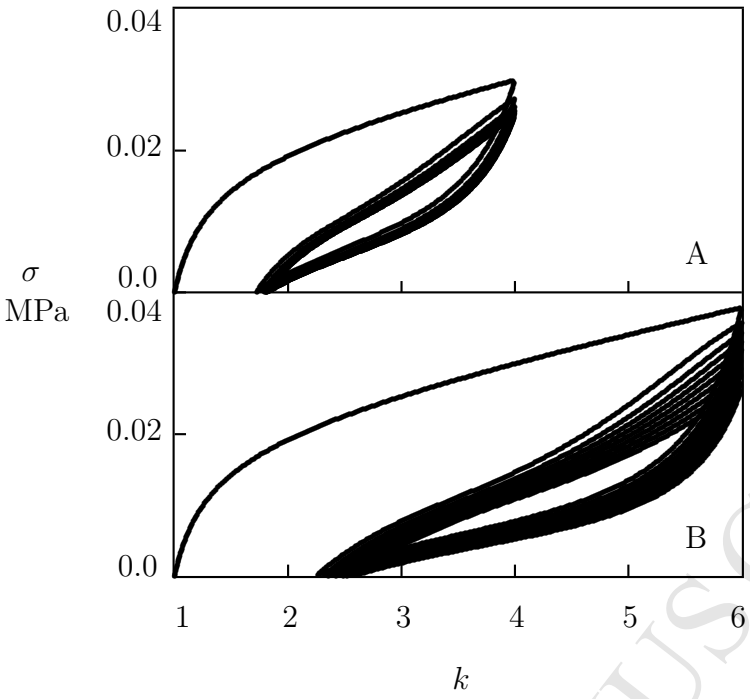

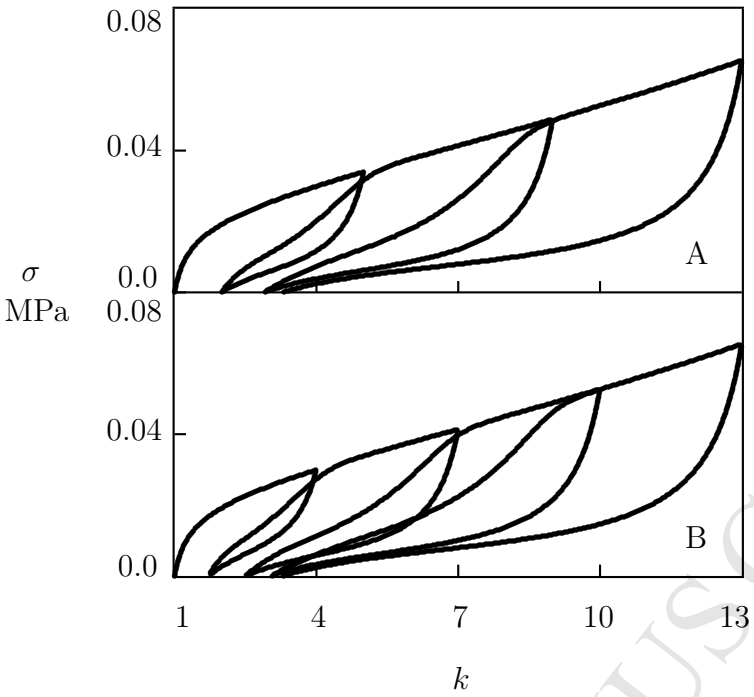

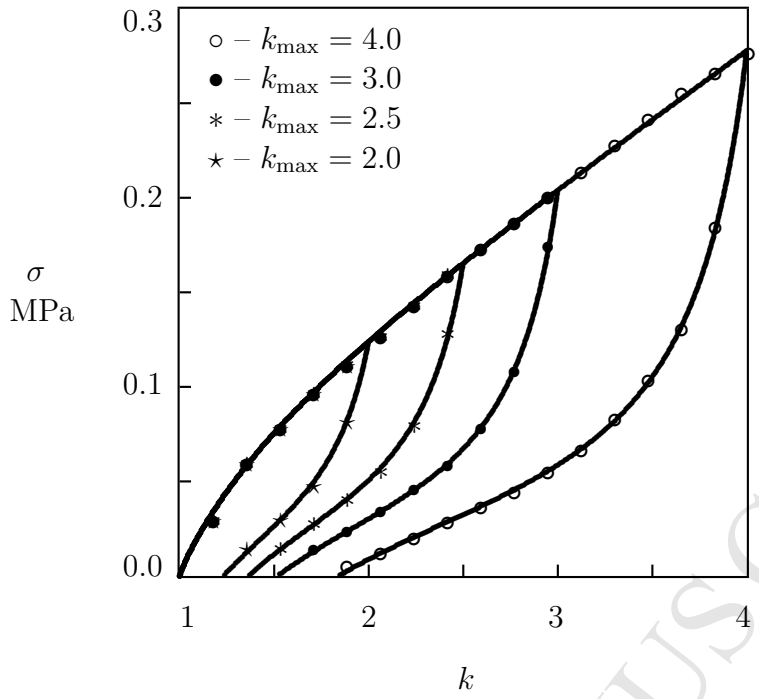

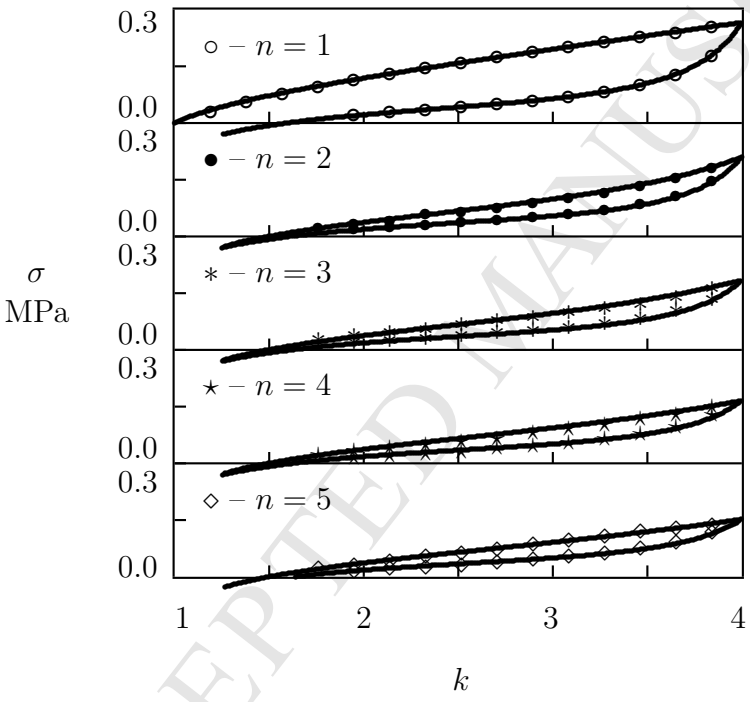

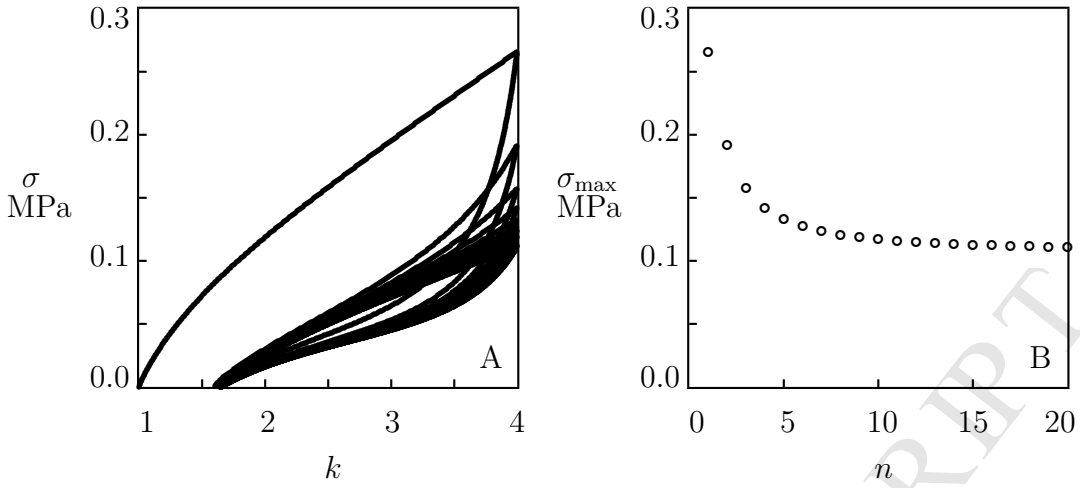

Mechanical response of double-network gels with dynamic bonds under multi-cycle deformation

A.D. Drozdov, J. deC. Christiansen

- A model is derived for the behavior of DN gels under multi-cycle deformation.
- Good agreement is revealed between observations and results of numerical analysis.
- The ability of the model to predict the Mullins effect is confirmed by simulation.